3-31-2023

THE FUNCTION OF TRANSPORT PROTEIN MFL1 IN ARABIDOPSIS THALIANA

Joseph Qian
Louisiana State University and Agricultural and Mechanical College

THE FUNCTION OF TRANSPORT PROTEIN MFL1 IN *ARABIDOPSIS THALIANA*

A Thesis

Submitted to the Graduate Faculty of the
Louisiana State University and
Agricultural and Mechanical College
in partial fulfillment of the
requirements for the degree of
Master of Science

in

The Department of Biological Sciences

by
Joseph Qian
B.S., Emory University, 2019
May 2023

ACKNOWLEDGEMENTS

First, I would like to thank my former advisor Paul South for letting me join his lab, providing me with the resources necessary for the experiments, and guiding me through the first two turbulent years of graduate school. Through him, I learned not only to think and present like a scientist but also to think critically, pay attention to details, and understand the critical importance of work-life balance. Despite my comical blunders and what life threw at him, his patience is an ability that I wish I even had a fraction of. I also would like to thank Dr. Naohiro Kato for taking me up in his lab on my third year and offering me irreplaceable editing and feedback on this thesis, Dr. David Vinyard for lending me some of his laboratory equipment and providing valuable insights on experimental design and presentation skills, and Dr. David Donze providing the yeast strains and guidance on how to grow and evaluate yeast results, Without them, my experiments would have never come to fruition. I would also like to thank my peers Nicholas Ferrari and Richard S. Garcia for helping me with my experiments while in the South lab, and Mary B. Rollins for helping me with making sure we all had our ingredients and reactants as well as providing insight into taking care of my experimental plants.

As for the friends that helped me fight through this difficult time, there were many, but for the notable ones, thank you Jeff Vannoppen and Andrei Moţ for providing invaluable technical support and appeasing the machine spirit. Thank you, André Santo, for keeping me on track and strongly reminding me that I need to take care of myself.

Finally, to Tom Bilak, from performing miracles to making sure I am all right every morning; you have given me hope and kept me safe from my demons for the past 2 years. I just hope that you will find the spark that burns away the shackles of depression so that you will find life worth living again before it is too late.

TABLE OF CONTENTS

LIST OF FIGURES

ABSTRACT

Photosynthesis serves as the primary process for plants to synthesize ATP and sugar molecules, however, this reaction requires many cofactors such as heme, plastoquinone, and iron-sulfur clusters to assist in energy gathering and electron transfer steps. Many of these require trace metals, such as iron, to cross across the chloroplast membranes and be incorporated into proteins and other organic molecules to form useable cofactors. The light-independent reactions of photosynthesis are also inefficient, with up to 25% of the photosynthetic energy wasted to metabolize the toxic waste product glycolate. The cellular logistics of both photorespiration and iron transport have been studied, but the transport proteins responsible for moving the reactions and products in and out of the chloroplast are not fully characterized. Although significant transporters such as permease in chloroplast 1 (PIC1), responsible for transporting iron, and plastidic glycolate glycerate transporter (PLGG1), responsible for transporting glycerate and glycolate in the chloroplast are well studied, other auxiliary transporters may still play a role in transporting molecules in and out of the chloroplast. This thesis attempts to understand the role of a poorly understood transporter, mitoferrin-like transporter (MFL1), in *Arabidopsis thaliana* within the chloroplast using three approaches: bioinformatics to predict its likely function; Golden Gate cloning to construct plasmids into both wild type *A. thaliana* and MFL1 deficient *A. thaliana* to observe the physiological effect under high, ambient, and low CO_2 conditions; and expressing the gene *mfl1* into *Saccharomyces cerevisiae* to determine its growth rate in conditions lacking iron and conditions lacking fermentable sugars. Experimental results suggest that MFL1 may play a role in transporting the molecule *S*-adenosyl methionine into the chloroplast. This study may provide insight into

discovering more transport proteins responsible for shuttling molecules in and out of the chloroplast to maintain the complex machinery for photosynthesis.

CHAPTER 1. BACKGROUND INFORMATION

1.1. Overview of Photosynthesis

Photosynthesis is a two-step chemical process where carbon dioxide and water are converted into sugar and oxygen using light energy (Arnon, 1971) (Figure 1.1).
Initially, light energy is absorbed by the light-harvesting complex antennae complex, which includes accessory pigments such as chlorophyll b, carotenoids, and xanthophylls (Meneghin et al., 2018; Pascal et al., 2005). This increases the energy level of an electron within the pigment molecule, and it is transferred to the next pigment molecule through resonance energy transfer. The energy transfer eventually reaches a group of chlorophyll molecules (P680) that utilize the energy to excite an electron and transfer them to an electron carrier plastoquinone (PQ) to eventually form reduced plastoquinol (PQH_2) (Amesz, 1973; Rabinowitch, 1957). Two water molecules are broken down into four protons and an oxygen molecule within photosystem II's water-oxidizing complex (Arnon, 1971). The hydrogen ions are pumped into the thylakoid space while the electrons from the split water molecules are energized and stored in PQH_2.

PQH_2 then gets transferred to the cytochrome b_6f complex where $4H^+$ are pumped into the thylakoid lumen and the electrons are transformed through a series of heme molecules and iron-sulfur complex molecules into plastocyanin (Kurisu et al., 2003). The plastocyanin then travels to photosystem I, which couples with another antenna complex. The electrons are then excited into a higher energy state in a pair of chlorophyll molecules sensitive to a wavelength of 700 nm. These electrons are then transferred into the molecule ferredoxin (Andersen et al., 1992). The electrons in ferredoxin are then either transferred to $NADP^+$ via ferredoxin-$NADP^+$ reductase or they are then transferred to the cytochrome b_6f complex for cyclic electron flow. The buildup of H^+ in the thylakoid lumen is used to propel ATP synthase to make ATP by

making the H^+ enter the motor assembly and then exit after completing one revolution (Steinberg-Yfrach et al., 1998).

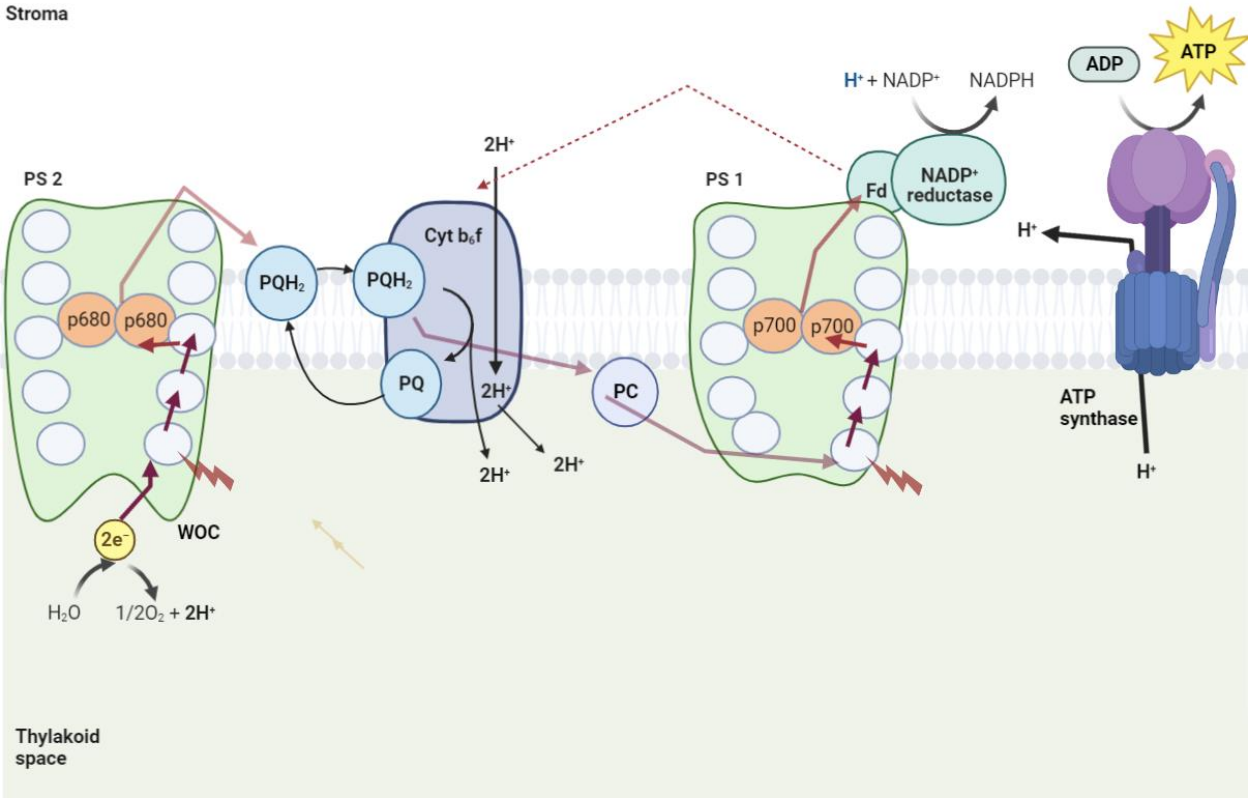

Figure 1.1. Overview of the light cycle of photosynthesis. A simplified diagram of where electrons travel after being removed from a water molecule in the light reaction of photosynthesis. PS 2: photosystem II, PS 1: photosystem I, WOC: water oxidizing complex, PQ: plastoquinone, Cyt b_6f: cytochrome b_6f, PC: plastocyanin, Fd: ferredoxin, Adapted from "Light-dependent reactions of photosynthesis", by BioRender.com (2023). Retrieved from https://app.biorender.com/biorender-templates.

The ATP and NADPH produced during the light cycle are then utilized in the C3 cycle (Figure 1.2). In the first step, three molecules of carbon dioxide (CO_2) are combined with three molecules of ribulose-1,5-bisphosphate (RuBP) to form six molecules of 3-phosphoglycerate by the enzyme ribulose-1,5-bisphosphate carboxylase (RuBisCO) present on the chloroplast stroma (Bassham, 2005). The enzyme phosphoglycerate kinase (PGK 1) then utilizes six molecules of ATP to transform six molecules of 3-phosphoglycerate into six molecules of 1,3-bisphosphoglycerate (Bassham, 2005). Finally, the enzyme glyceraldehyde-3-phosphate dehydrogenase (GAPDH) uses 6 molecules of NADPH to convert the six molecules of 1,3-

bisphosphoglycerate into glyceraldehyde-3-phosphate (G3P) (Bassham, 2005). After two triplicate cycles of the C3 reaction, two molecules of G3P are exported to the cytoplasm and utilized to form hexose sugars. One of the G3P molecules is transformed into dihydroxyacetone phosphate (DHAP) via triose phosphate isomerase (Bassham, 2005) and then both molecules are made into fructose-1,6-bisphosphate by the enzyme fructose bisphosphate aldolase (Bassham, 2005).

To regenerate the three molecules of ribulose-1,5-bisphosphate, one molecule of G3P from the first carbon fixation reaction is converted into one DHAP molecule by triose phosphate isomerase. Then, the G3P and DHAP molecules are combined to form fructose-1,6-bisphosphate (FBP) by the enzyme fructose bisphosphate aldolase (Marsh & Lebherz, 1992). Transketolase removes two carbons from FBP to form erythrose-4-phosphate (E4P). The 2-carbon molecule is added to one molecule of G3P from the second carbon fixation event to form xylulose-5-phosphate (Xu5P). The second G3P from the second carbon fixation event is then converted to DHAP and added to E4P to form sedoheptulose-1,7-bisphosphate (7C) by aldolase. One phosphate molecule is released from 7C by the enzyme sedoheptulose-bisphosphatase to form sedoheptulose-7-bisphosphate (S7P). A 2-carbon molecule is removed from S7P by the enzyme transketolase to form ribose-5-phosphate (R5P), and the 2-carbon molecule is attached to the final G3P to form another Xu5P. R5P is converted into ribulose-5-phosphate (Ru5P) by ribose-5-phosphate isomerase (Rpi) and the two Xu5P are converted into Ru5P by the enzyme ribulose-5-phosphate epimerase (L-Ru5P-4 epimerase) (Bassham, 2005). In the final step, Ru5P is then converted back into RuBP by the addition of phosphate by ATP by the enzyme ribulose-5-phosphate kinase (PRK) (Porter et al., 1986).

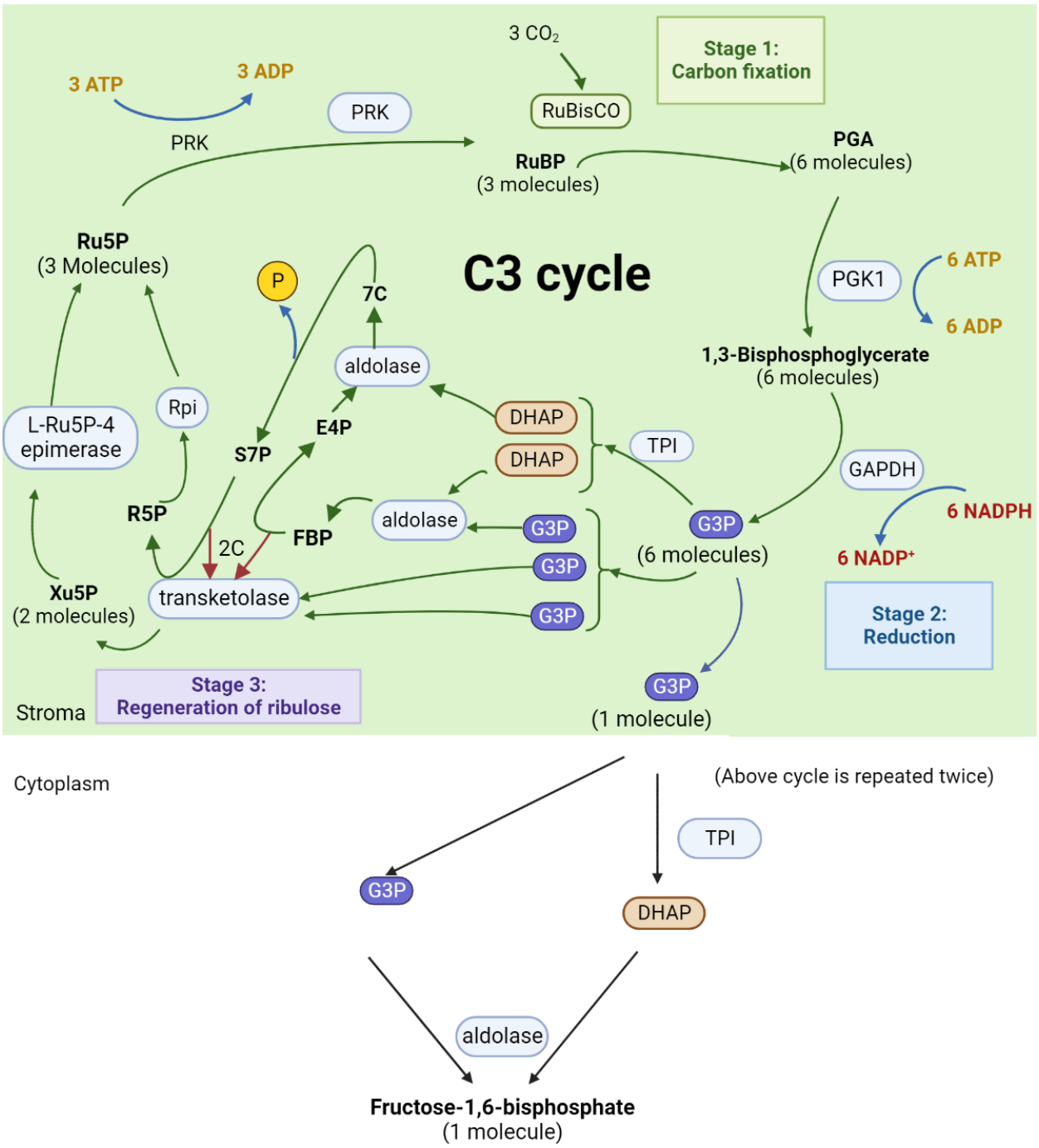

Figure 1.2. Overview of the C3 reaction of photosynthesis. A simplified diagram of the glucose production in the light-independent reactions. RuBP: ribulose-1,5-bisphosphate, PGA: 3-phosphoglycerate, PGK 1: phosphoglycerate kinase, GAPDH: glyceraldehyde-3-phosphate dehydrogenase, G3P: Glyceraldehyde-3-phosphate, DHAP: dihydroxyacetone phosphate, FBP: fructose-1,6-bisphosphate, E4P: erythrose-4-phosphate, 7C: sedoheptulose-1,7-bisphosphate, S7P: sedoheptulose-7-bisphosphate, R5P: ribose-5-phosphate, Xu5P: xylulose-5-phosphate, Rpi: ribose-5-P isomerase, Ru5P: Ribulose-5 phosphate, L- Ru5P-4 epimerase: ribulose-5-phosphate epimerase, PRK: ribulose-5-phosphate kinase. Red arrows indicate the transfer of 2-carbon molecules. Created with BioRender.com.

1.2. Overview of Photorespiration

The waste product oxygen from the light reactions often enters RuBisCO in the Calvin-Benson cycle and produces the 2-carbon product 2-phosphoglycolate (2PG) (Tabita et al., 2007) (Figure 1.3). 2PG inhibits many enzymes within the photosynthesis reactions such as triose phosphate isomerase and phosphofructokinase. (Anderson, 1971; Flügel et al., 2017; Kelly & Latzko, 1976). To recycle 2PG, it is first dephosphorylated into glycolate with the enzyme 2-Phosphoglycolate phosphatase (PGLP) (Timm et al., 2019), then exported out of the chloroplast by the plastidic glycolate glycerate transporter (PLGG1) and the bile acid sodium symporter 6 (BASS6) (Pick et al., 2013; South et al., 2017).

Glycolate then enters the peroxisome where it is oxidized into glyoxylate via the enzyme glycolate oxidase (GO) (Zelitch et al., 2009) and glyoxylate is then converted into glycine by the enzyme glyoxylate glutamate aminotransferase (GGAT) (Igarashi et al., 2003). Glycine is transported into the mitochondria, where ammonia and carbon dioxide are removed by glycine decarboxylase (GLDC) and NADH, then another glycine is combined to form the 3-carbon serine molecule by the enzyme serine hydroxymethyltransferase (SHMT) (Beckmann et al., 1997).

Serine then enters the peroxisome again and is converted into hydroxypyruvate by the enzyme serine-glyoxylate aminotransferase (SGAT) (Liepman & Olsen, 2003). Hydroxypyruvate is then converted to glycerate via reduction by NADH with the enzyme hydroxy pyruvate reductase (HPR) (Timm et al., 2008). The glycerate can then reenter the chloroplast by PLGG1 and enter the Calvin-Benson cycle. This process produces CO_2 and uses ATP, which translates to a loss of up to 25% of photosynthetic output in a plant performing photorespiration (Peterhansel et al., 2010).

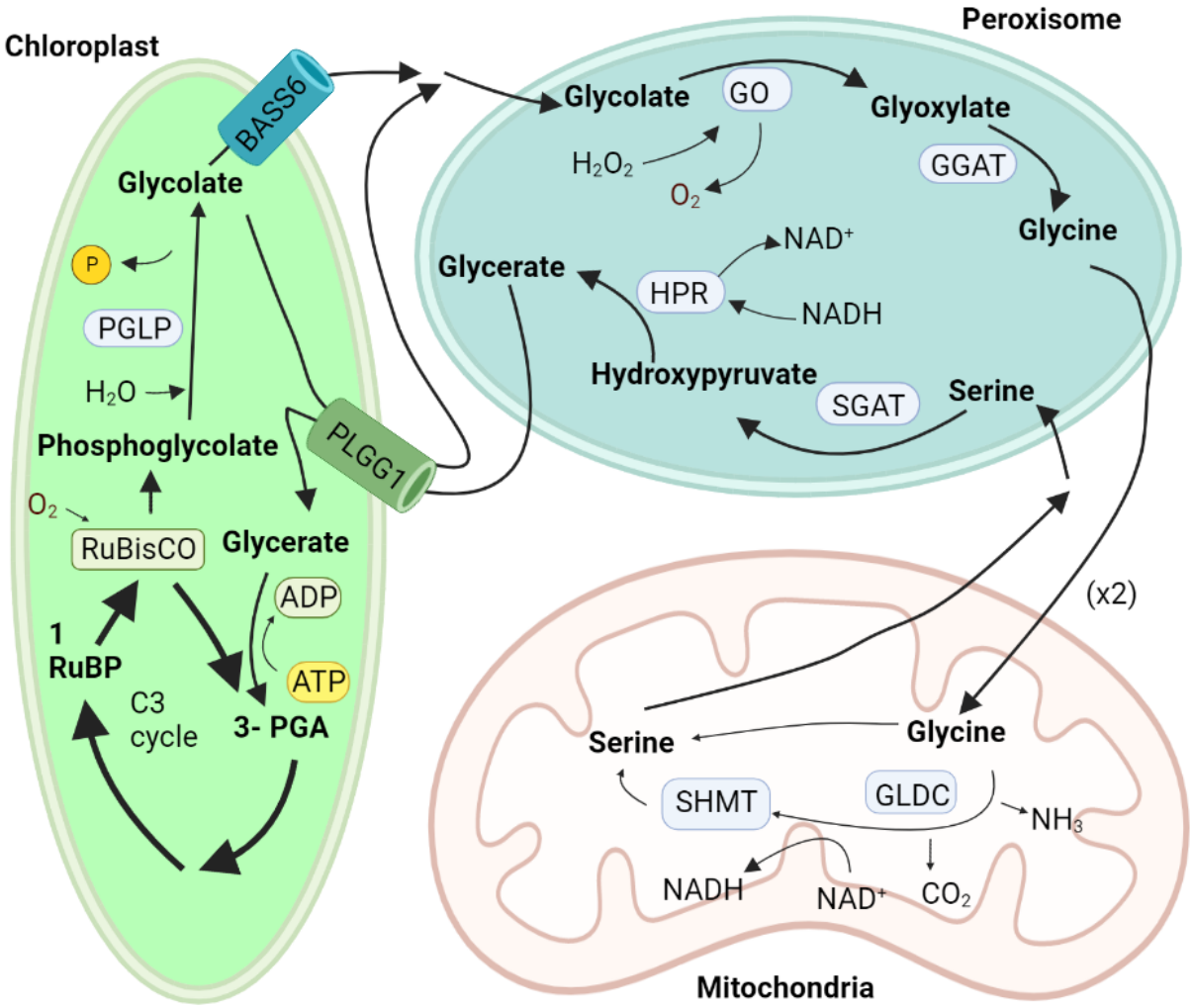

Figure 1.3. Overview of Photorespiration. A simplified diagram of the photorespiration reaction. PGLP: 2-Phosphoglycolate phosphatase, PLGG1: plastidic glycolate glycerate transporter, BASS6: bile acid sodium symporter six, GO: glycolate oxidase, GGAT: glyoxylate glutamate aminotransferase, GLDC: glycine decarboxylase, SHMT: serine hydroxymethyltransferase, SGAT: serine-glyoxylate aminotransferase, HPR: hydroxy pyruvate reductase. 3-PGA: 3-phosphoglycerate, created with BioRender.com.

1.3. Iron utilization in the chloroplasts

Since the light reactions require trace metals such as iron for the election transfer functions (Zhang et al., 2004), nitrate assimilation (Campbell & Redinbaugh, 1984), and as a cofactor for iron-sulfur cofactor functions (Hall et al., 1975), plants will need a way to assimilate, transport, store, and utilize iron in the chloroplast (Figure 1.4). First, iron (III) (Fe^{3+}) is reduced to iron (II) (Fe^{2+}) by the enzyme ferric chelate oxidoreductase (FRO7) (Solti et al.,

2014). The reduced iron is then transported into the stroma of the chloroplast by the transporter permease in chloroplast 1 (PIC1) (Duy et al., 2007). Once Fe^{2+} enters the stroma, there are three known pathways where it can be assimilated and used in the chloroplast. One pathway is where Fe^{2+} is incorporated into ferritin to be stored for later use and protects the plant against oxidative damage (Ravet et al., 2009). The other pathway for Fe^{2+} to be used in the chloroplast is incorporated into heme assembly. Here, Fe^{2+} is combined with frataxin to form a Fe-frataxin complex and used as an ingredient in the last step of heme synthesis, where the iron is added to a protoporphyrin IX molecule to form a heme via the enzyme ferrochelatase (Woodson et al., 2011). Another pathway where iron is utilized in the chloroplast is the iron-sulfur synthesis pathway. In this pathway, a sulfur molecule is first removed from cysteine by pyridoxal-L-phosphate (PLP)-dependent cysteine desulfurase (NFS2) and quinolinone synthase (SUFE1-3) enzyme complex (Pilon-Smits et al., 2002). The resulting alanine is removed, and the sulfur is carried to a scaffold protein complex made from four subunits: one b subunit (SUFB), two c subunits (SUFC), and one d subunit (SUFD)(Hu et al., 2017). Once ATP binds to one of the SUFC subunits, it induces a conformational change within the complex that is energetically favorable for Fe-S formation (Hirabayashi et al., 2015). In addition to ATP, $FADH_2$ is also added to the scaffold complex to reduce the Fe^{3+} from the Fe-frataxin complex into Fe^{2+} for it to bind to the sulfur to form a Fe-S cluster (Saini et al., 2010).

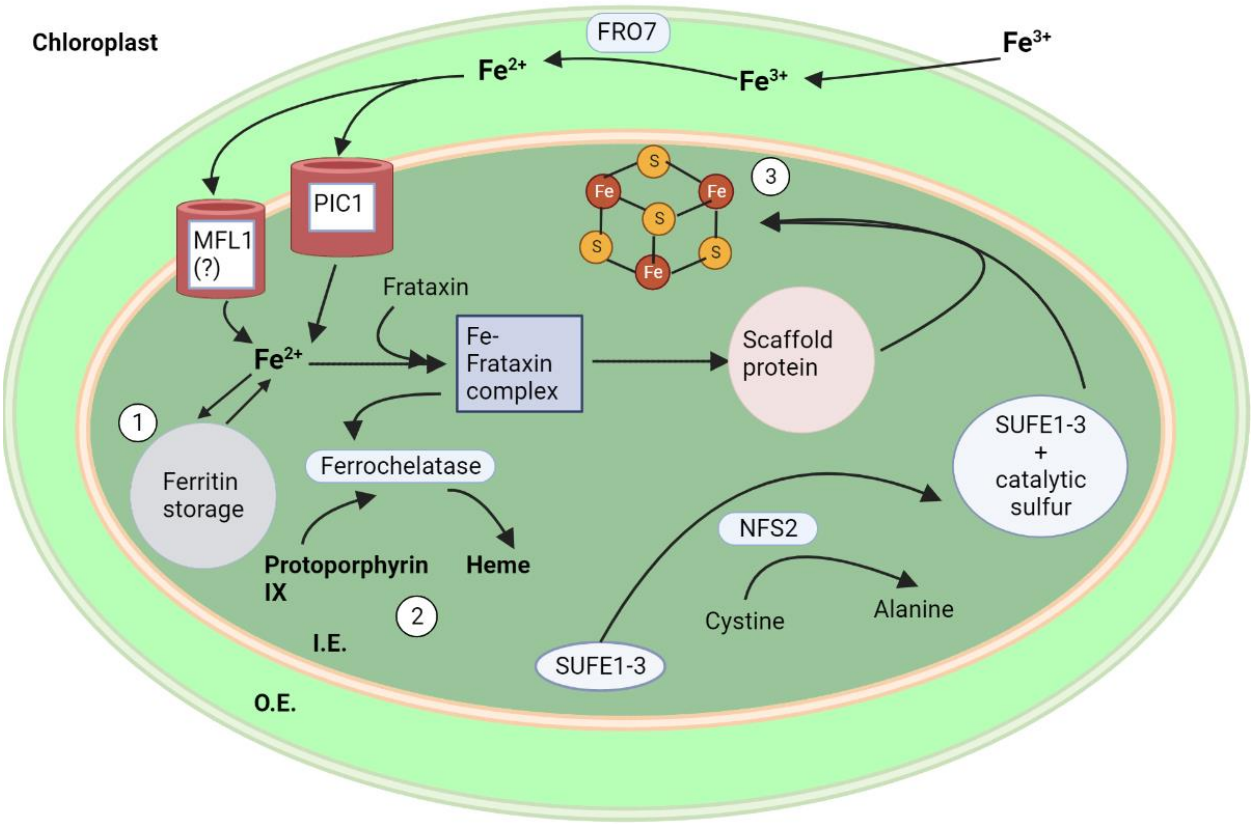

Figure 1.4. Overview of iron utilization in plants. A basic pathway of an iron metabolic pathway in the chloroplast, FRO7: ferric reductase oxidase, O.E.: outer envelope, I.E.: inner envelope, PIC1: permease in chloroplast 1, MFL1: mitoferrin-like transporter in A. thaliana, SUFE1-3: quinolinone synthase enzyme complex, created with BioRender.com.

CHAPTER 2. IDENTIFYING THE FUNCTION OF MFL1

2.1. Introduction.

A mitoferrin-like transporter in *A. thaliana* (MFL1) is hypothesized to play a role in transporting iron between the chloroplast, cytosol, and photorespiration. Previous literature has suggested that it serves as a ferric ion transporter with the chloroplast's inner membrane (Tarantino et al., 2011). (Fig 1.4.). However, preliminary bioinformatic modeling and phylogenetic lineage modeling of MFL1, suggest that MFL1 could be an *S*-adenosyl methionine (SAM) transporter (Fig 2.1., Fig 2.2.).

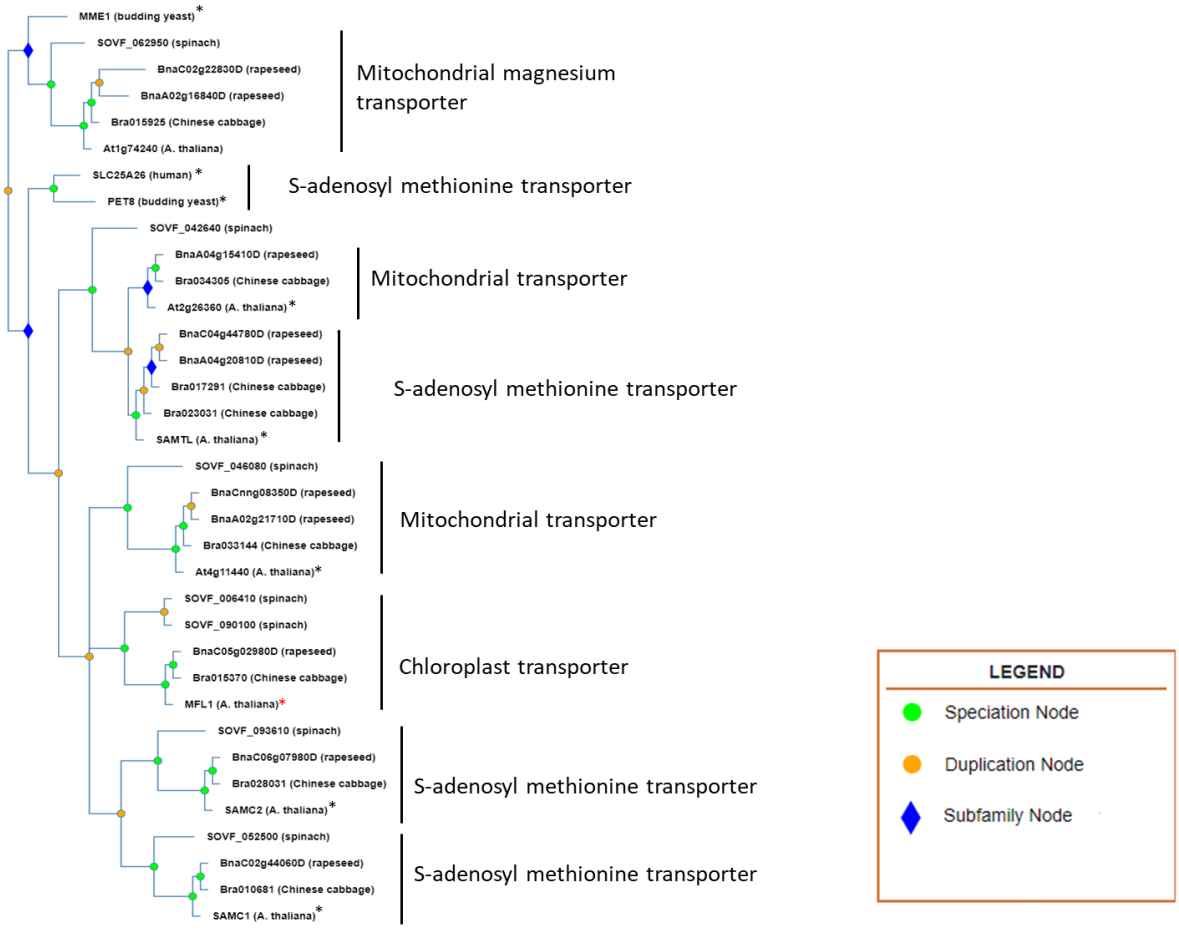

Figure 2.1. The phylogeny of MFL1 is similar to other S-adenosyl transporters. Predicted phylogenetic tree of MFL1 based on protein alignments. an asterisk indicates the known function, and a red asterisk indicates MFL1.

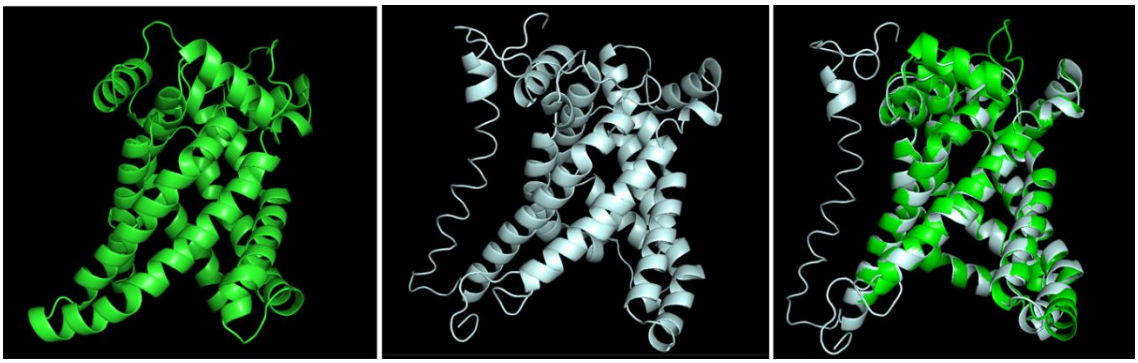

Figure 2.2. The predicted 3D structure of MFL1 is similar to a known chloroplast S-adenosyl methionine transporter**.** 3D model of MFL1 in *A. thaliana* (left). 3D model of SAMC1 in *A. thaliana* (center). 3D model overlays of MFL1 and SAMC1 (right).

SAM is an important reactant in almost all organisms. It is chiefly used as a methyl group donor for DNA, RNA, and protein methylation (Pintard et al., 2002; Santamaría et al., 2003), however, since it is synthesized in the cytosol, it needs to be imported into organelles such as mitochondria and chloroplasts to be used as important methylation cofactors for mitochondrial proteins involved in the Krebs cycle (Ravanel et al., 2004; Santamaría et al., 2003).

This research aims to identify the biological function of MFL1 in plants. To accomplish this, we did experimentations including placing MFL1 knockdown plants in a high CO_2 environment to see if a high CO_2 environment would rescue the knockdown plant and measuring the non-photochemical quenching abilities of the MFL1 knockdown plants as well as using yeast model organisms to estimate what substrate MFL1 transports.

2.2. Materials and Methods.

2.2.1. Phylogenetic lineage modeling

For the phylogenic lineage modeling, we used the PhyloGenes phylogenetic tree builder to determine MFL1's position in the PANTHER gene family using the GIGA algorithm (Zhang et al., 2020). The branch length was calculated based on differences in the ancestral sequence (Thomas, 2010), and the tree was pruned to include *A. thaliana* and its close relatives along with

the closest human and *S. cerevisiae* protein counterparts. The downloaded tree was modified using MS Paint.

2.2.2. Prediction 3D modeling of MFL1 and SAMC1

For our prediction 3D modeling of MFL1 and SAMC1, we obtained both the MFL1 and SAMC1 sequences from The Arabidopsis Information Resource (TAIR). The sequences were then inputted into the Phyre 2 modeling software browser under normal mode (Kelley et al., 2015). The resulting .pdb files were then opened and visually compared in PyMOL for sequence and structure similarity.

2.2.3. Plant lines and growth conditions

Mutant *mfl1-2* lines were obtained at ABRC (SALK_007617C), and mutant plant lines were made by inserting the construct plasmids into WT Col-0 plants and *mfl1-2* lines using a modified floral dip method (Zhang et al., 2006). Specifically, an *Agrobacterium tumefaciens* strain was transformed to carry the construct of interest, and a single colony of the transformed bacteria was inoculated overnight at 28°C in a 5 mL LB culture with an antibiotic to select for the binary plasmid. The starter culture was then diluted 1:100 and grown overnight. On the third day, when the cultures have grown to mid-logarithmic or stationary phase, the cells were centrifuged for 10–20 min at room temperature at approximately 5500g. The cell pellets were resuspended in an equal volume of freshly made 5% sucrose solution to achieve O.D.600 = 0.8. *A. thaliana* flowers were then dipped in 100 mL of the sucrose *A. tumefaciens* solution. The flowers were then dried and left overnight in a dark place, then placed back into a Percival growth chamber and grown at a 12-hour day-night cycle starting at 9 am and at a temperature of 22°C at day and 18°C at night. The light level was set to 37% (150 -180 µmol m^{-2} s^{-1}).

2.2.4. Plasmid constructs

A. thaliana plasmid constructs were made with the Golden Gate method (Weber et al., 2011). For the level 1 plasmids, the MFL1 promoter, open reading frame, and terminator were obtained by sequences from TAIR. The overexpression constructs were made with the p35 promoter, the MFL1 open reading frame, a C-terminal eGFP tag, and the MFL1 native terminator (Supplementary Fig.1.). The complementation construct was made with the MFL1 promoter, the MFL1 open reading frame, a C-terminal 3xFLAG tag, and the MFL1 native terminator (Supplementary Fig.2.). The plant level one plasmids were assembled by preparing the plasmid backbone (EC47742) (https://www.ensa.ac.uk/) and the desired linear inserts in a 1:3 molar concentration ratio, 2 µL of 10X T4 buffer (50 mM Tris-HCl, 10 mM $MgCl_2$, 1 mM ATP, 10 mM DTT, pH 7.5 at 25°C at 1X concentration), 1 µL of 10,000 units of T4 ligase, (a concentration of 400,000 cohesive end units/mL with 10 mM Tris-HCl, 50 mM KCl, 1 mM DTT, 0.1 mM EDTA, 50% glycerol, pH 7.5 at 25°C as the storage buffer), 1 µL of Bsa1 (a concentration of 20,000 units/mL with 10 mM Tris-HCl, 200 mM NaCl, 1 mM DTT, 0.1 mM EDTA, 200 µg/mL Recombinant Albumin, 50% glycerol, and pH 7.4 at 25°C as the storage buffer). The final reaction volume was filled to 20 µL by pure water and incubated at 37°C for 5 minutes, then 16°C for 5 minutes, and these two steps were repeated 30 times, after which the tube was incubated at 50°C for 5 minutes, 80°C for 5 minutes, and finally held at 12°C.

The plant level 2 plasmids were prepared with the insert plasmid EC15324 and one of the constructed level 1 plasmids along with end linker plasmid 2 (ELE-2) (Supplemental figure 3.) (https://www.ensa.ac.uk/). The plant level 2 plasmids were assembled by preparing the plasmid backbone EC50507 (https://www.ensa.ac.uk/) and the desired level 1 plasmid in a 1 to 3 molar concentration ratio, 2 µL of 10X T4 buffer (50 mM Tris-HCl, 10 mM $MgCl_2$, 1 mM ATP, 10

mM DTT, pH 7.5 at 25°C at 1X concentration), and 1 µL of 10,000 units of T4 ligase, (a concentration of 400,000 cohesive end units/mL with 10 mM Tris-HCl, 50 mM KCl, 1 mM DTT, 0.1 mM EDTA, 50% glycerol, pH 7.5 at 25°C as the storage buffer.) and 1 µL of Bpi1/Bbs1. (a concentration of 10,000 units/mL with 10mM Tris-HCl, 300 mM NaCl, 1 mM DTT, 0.1 mM EDTA, 500 µg/mL Recombinant Albumin 50% glycerol, and pH 7.4 at 25°C as the storage buffer.) The final reaction volume was filled to 20 µL by pure water and incubated at 37°C for 5 minutes, then 16°C for 5 minutes, and these two steps were repeated 30 times, after which the tube was incubated at 50°C for 5 minutes, 80°C for 5 minutes, and finally held at 12°C.

Yeast plasmid constructs were created using the MoClo yeast toolkit method (Lee et al., 2015), the yeast-specific promoters and terminators were obtained with the MoClo kit, and the open reading frames for *FTR1* and *SAM5* were obtained through yeastgenome.org. The *PIC1* and *MFL1* open reading frame was obtained by TAIR. The yeast plasmids were assembled by putting the plasmid backbone (Pytk083) against the inserts in a 1: 3 molar concentration ratios. The inserts are the connection L1 (Pytk003), a combination of promoters, coding regions, connection R1 (Pytk067), ADH1 terminator (Pytk053), URA3 (Pytk074), and Cen6/Ars4 (Pytk081). For the iron complementation assay, the predicted FTR1 signal peptide coding region was added to *MFL1* and *PIC1*genese, while for the SAM complementation assay the predicted SAM5 signal peptide coding region was added to the *MFL1* gene (Supplementary Figure 4, Supplementary Table 2.), Other enzymes and reactants added include 1.5 µL of 10X T4 buffer (50 mM Tris-HCl, 10 mM $MgCl_2$, 1 mM ATP, 10 mM DTT, pH 7.5 at 25°C at 1X concentration), 1 µL of 10,000 units of T4 ligase, (a concentration of 400,000 cohesive end units/mL with 10 mM Tris-HCl, 50 mM KCl, 1 mM DTT, 0.1 mM EDTA, 50% glycerol, pH 7.5 at 25°C as the storage

buffer), and 1 µL of 10,000 units of Bsa1 (a concentration of 20,000 units/mL with 10mM Tris-HCl, 200 mM NaCl, 1 mM DTT, 0.1 mM EDTA, 200 µg/mL Recombinant Albumin 50% glycerol, and pH 7.4 at 25°C as the storage buffer). The final reaction volume was adjusted to 20 µL with pure water and incubated at 42°C for 2 minutes, then 16°C for 5 minutes, and these two steps were repeated 40 times, after which the tube was incubated at 60°C for 10 minutes, 80°C for 10 minutes, and held at 12°C. All constructs were evaluated by PCR using specific primers (Supplementary Table 1.) to verify accuracy.

2.2.5. Plant genomic extraction and PCR

A modified protocol (Edwards et al. 1991) was used, specifically, *A. thaliana* genomic extraction was performed by crushing a piece of leaf tissue with 500 µL of extraction buffer (200 mM Tris-HCl, 250 mM NaCl, 25 mM EDTA, 0.5% SDS). At a pH of 7.5, the mixture was then centrifuged at 10,000 RPM for 5 minutes, then the supernatant was extracted and added with the same amount of 100% isopropanol. The mixture was then centrifuged at the same RPM for 5 minutes and the pellet was resuspended in 50 µL of pure water. 1 µL of this genomic DNA solution was then added to a PCR tube along with 12.5 µL of OneTaq master mix (20 mM Tris-HCl, 22 mM KCl, 22 mM NH_4Cl, 1.8 mM $MgCl_2$, 5% glycerol, 0.05% Tween 20, 0.06% IGEPAL CA-630, 0.2 mM dNTP, 25 units/mL OneTaq® DNA Polymerase, and pH 8.9 at 25°C as the storage buffer) and 0.5 µL of 10 µM primers (supplementary table 1.).

2.2.6. RNA extraction

RNA extraction was done by following the MACHEREY-NAGEL RNA Extraction Kit protocol. Leaf tissue was frozen with liquid nitrogen, then crushed and mixed with 350 µL Buffer RP1 (50% guanidinium thiocyanate, 50% pure water) and 3.5 µl β-mercaptoethanol. The mixture was then put in a violet Nucleospin lysate filter spin column provided within the kit and

centrifuged at 11,000 RPM for one minute to remove cell debris. The lysate filter was then washed with 350 µL of 70% ethanol. The resulting lysate was then placed on the light blue Nucleospin RNA isolation filter spin column and put at the same RPM for 30 seconds. After isolating the RNA, 350 µL of the MBD (20% ethanol, 10% guanidinium thiocyanate, and 70% pure water) was added and the mixture was centrifuged at the same RPM for 1 minute. 95 µL of rDNAse was added and incubated for 15 minutes. 200 µL of RA2 buffer (35% ethanol, 45% guanidinium thiocyanate, 20% pure water) was added and the mixture was centrifuged at 11,000 RPM for 30 seconds. The samples were then washed with 600 µL of working RA3 solution (1-part RA3 concentrate and 4 parts 100% ethanol) and centrifuged at 11,000 RPM for 30 seconds, then washed with 250 µL of working RA3 solution and centrifuged at 11,000 RPM for 2 minutes, then finally washed with 600 µL of working RA3 solution and centrifuged with 11,000 RPM for 30 seconds. Finally, RNAse-free H_2O was used to elute the RNA from the filter and centrifuged at the same RPM for 1 minute, the RNA was then stored at -60°C for later use.

2.2.7. RNA reverse transcription and PCR

RNA reverse transcription protocol was used by Qantinova RNA reverse transcription kit, specifically, 2 µL of the genomic DNA removal mix was added to 15 µg of RNA and pure water to make a reaction volume of 15 µL. The mixture was then incubated at 45°C for 2 minutes and placed on ice immediately afterward. 1 µL of reverse transcription enzyme and 4 µL of reverse transcription mix was added and the mixture was then incubated at 25°C for 3 mins, 45°C for 20 minutes, and finally at 85°C for 5 minutes. 1 µL of this cDNA solution was then added to a PCR tube along with 12.5 µL of OneTaq master mix and 0.5 µL of 10 µM primers (supplementary table 1.).

2.2.8. Growth assay

Six 3.5-inch pots were filled with soil (Fafard Sungro #3B) that was spread even at the surface. Two plants of each type were planted at the opposite corners of each pot, totaling 12 plants of each line. The plants were placed into a Percival growth chamber and grown at a 12-hour day-night cycle starting at 9 am and a temperature of 22°C at day and 18°C at night. The light level was set to 37% (150 -180 µmol m^{-2} s^{-1}). The leaf area measurements started 7 days after planting and continued for the 9^{th}, 14^{th}, 16^{th}, 21^{st}, 23^{rd}, 28^{th}, and 30^{th} days after planting. The measurement was completed using the software "easy leaf Area" with a 4 cm^2 red paper square (Easlon & Bloom, 2014).

2.2.9. Yeast iron assays.

Saccharomyces cerevisiae strain BY4742 was obtained through Horizon Discovery Company. A colony of BY4742 was selected and transformed with the plasmids indicated. These transformed yeasts were then grown in a 5 mL culture overnight to achieve an OD between 0.2 and 1. Once the culture was at the desired OD, it was then serially diluted from 0.1, and 10 µL of the diluted culture was plated onto both the SC-URA control plate and the SC-URA with the iron chelator bathophenanthroline disulfonate (BPDS) at a concentration of 50 µM (Bashir et al., 2011). The culture was grown for 48 hours, and images were taken.

2.2.10. S-adenosyl methionine Yeast assays.

Strain BY4741 was grown as above and 10 µL of the diluted culture was plated onto both the SC-URA (Supplementary Table 3.) control plate and the SC-URA with the glucose replaced with D+ galactose (Marobbio et al., 2003). The culture was grown for 48 hours, and images were taken.

2.2.11. Non-photochemical quenching experiment.

The seeds of the study were soaked with a 50% by-volume bleach solution for 5 minutes then rinsed in sterile water, then the seeds were suspended in a 1% agar solution and kept at 4°C in the dark for 2 days. On the third day, the seeds were plated onto an MS plate, sealed with surgical tape, then kept in an 8-hour day cycle with 150 µmol m^{-2} s^{-1} of light with the temperature at 22°C in the day and 18°C in the night for 8 days. On day 9, before the day cycle starts, 3 replicate plates were placed in a 0% CO_2 environment, 2000 ppm high CO_2 environment, and ambient CO_2 environment, incubated for 12 hours, and plates were wrapped in foil to dark adapt. On day 10, plates were imaged using the NPQ protocol on a closed FluorCam FC 800-C (Photon System Instruments).

2.3. Results

First, we verified that *mfl1-2 A. thaliana* mutants previously isolated (Tarantino et al., 2011) have a T-DNA insert within the -63 position of the start codon of the *mfl1* gene (Fig 2.3.). Out of the 6 plants that tested positive for having the T- DNA insertion, plant number 2 was used for future experiments.

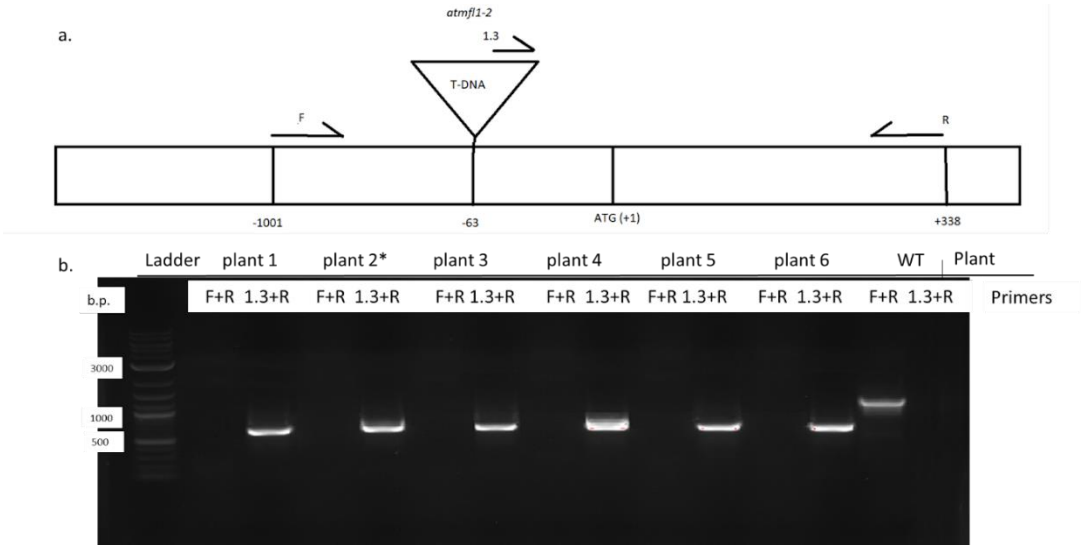

Figure 2.3. *mfl1-2* mutants have a T-DNA insertion in the promoter. *(*a.) mfl1 only has one exon and no introns, the T-DNA insert in *mfl1-2* is shown here, with F and R being the forward primer and reverse knockout verification primers and 1.3 being the T-DNA verification primer (Supplementary Table 1.). (b.) gel image of the PCR analysis verifying the T-DNA insertion in mfl1-2 mutants. plant 2 is used in further experiments as (*mfl1-2*). b.p.= base pairs.

We utilized endpoint-PCR to verify the presence of mfl1 mRNA transcripts within (Fig. 2.4.), however, there was a knockdown expression level of the mfl1 gene. The expressions of the violaxanthin de-epoxidase (VDE) gene, used as a control, were similar in both WT and *mfl1-2* mutants.

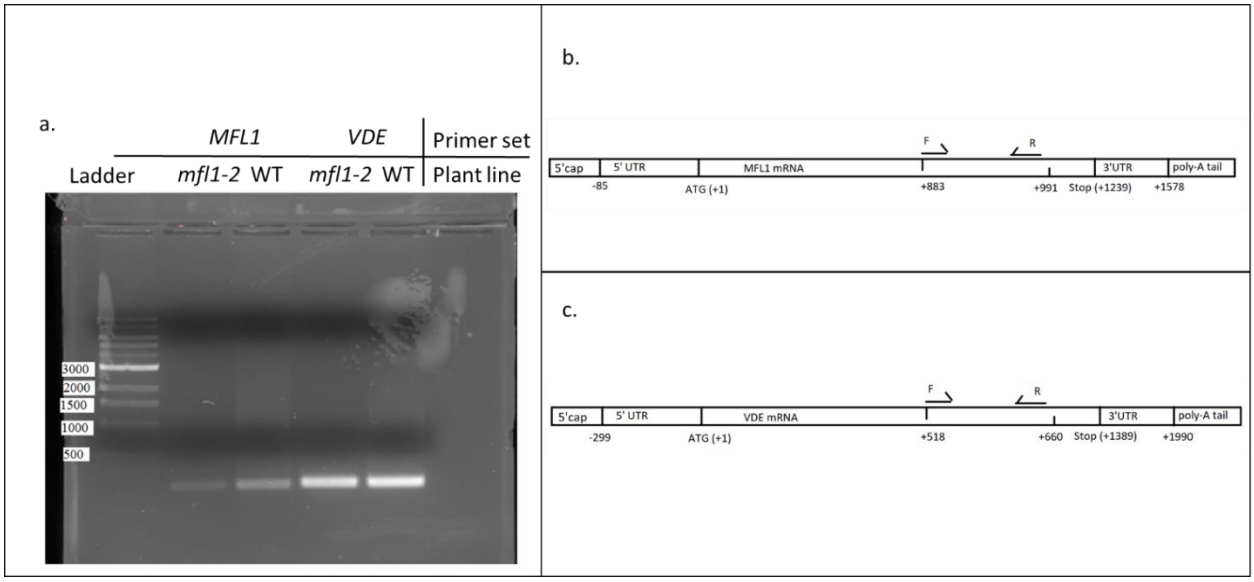

Figure 2.4. Mutant *mfl1-2* are knockdown mutants. *(*a.) Mutant knockdown mfl1-2 and wildtype *A. thaliana* (WT) endpoint PCR, with primers targeting the MFL1 (experimental), and Violaxanthin de-epoxidase (VDE) (control). (b.) Diagram of the MFL1 mRNA transcript, with primers attached, with F and R being the forward primer and reverse MFL1 mRNA transcript endpoint PCR primers (Supplementary Table 1.). (c.) Diagram of the VDE mRNA transcript, with primers attached, with F and R being the forward primer and reverse VDE mRNA transcript endpoint PCR primers (Supplementary Table 1.).

We generated transgenic *A. thaliana* in which a recombinant *mfl1* gene is overexpressed. To verify the overexpression, we did a genomic PCR on our transgenics (Fig. 2.5.). We confirmed that the molecular size of the overexpressed *mfl1* gene is larger than the native gene due to the addition of the eGFP gene tag in the 3' end. Plant number 4 had successfully integrated the recombinant *mfl1* into the genome and was used for future experiments.

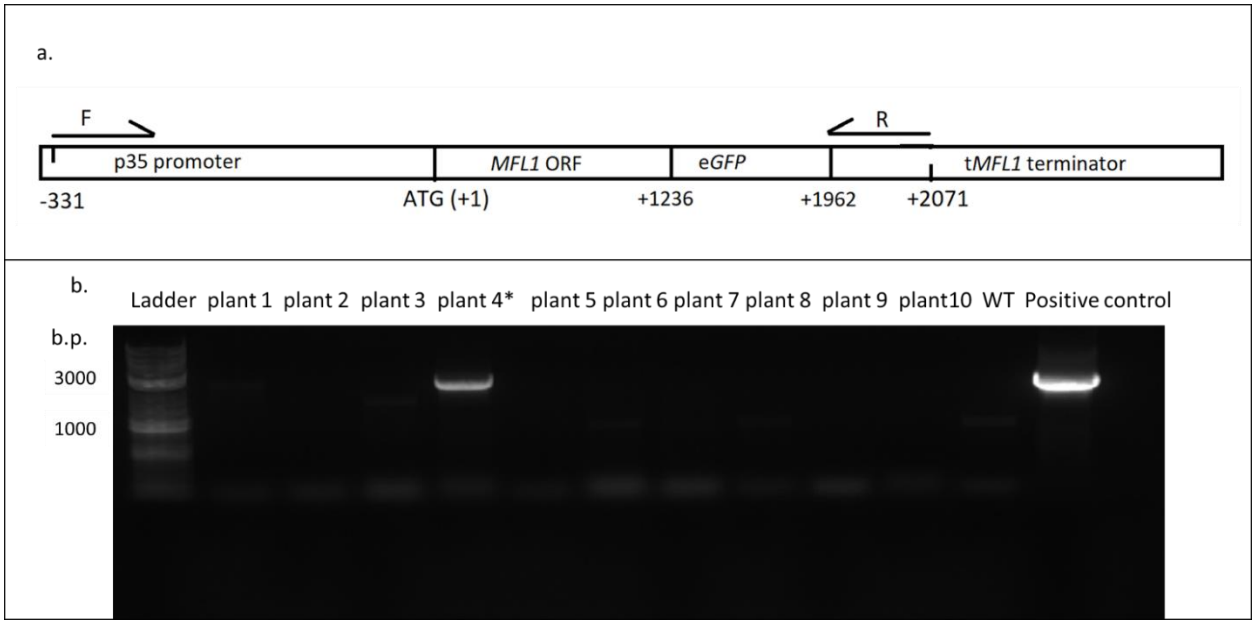

Figure 2.5. Genomic endpoint PCR verification that overexpressed MFL1 is made with a p35 promoter and an eGFP tag. (a.) Overexpressed *MFL1* has a P35 promoter, and the forward primer targets -331 bp upstream within that region, with F being the forward promoter p35 primer and R being the reverse *mfl1* gene primer (Supplementary Table 1.). (b.) gel image of the PCR analysis verifying the overexpression of *mfl1-2* mutants. The expected band size is 2402 b.p. Plant 4, marked with an asterisk (*) in the figure, is used in further experiments as (ox). The positive control is the p35 MFL1 overexpression plasmid (Supplementary Figure 1.).

We also generated complemented transgenic *A. thaliana* in which the *MFL1* gene knockout was rescued with the recombinant *MFL1* gene fused to the 3xFLAG tag. We did a genomic PCR on our transgenics (Fig. 2.6.). The complemented *MFL1* gene is 81 base pairs larger than the native gene due to the addition of the 3xFLAG gene tag in the 3' end. Out of the five plants transformed, Plant number 1 was used for the subsequent experiments.

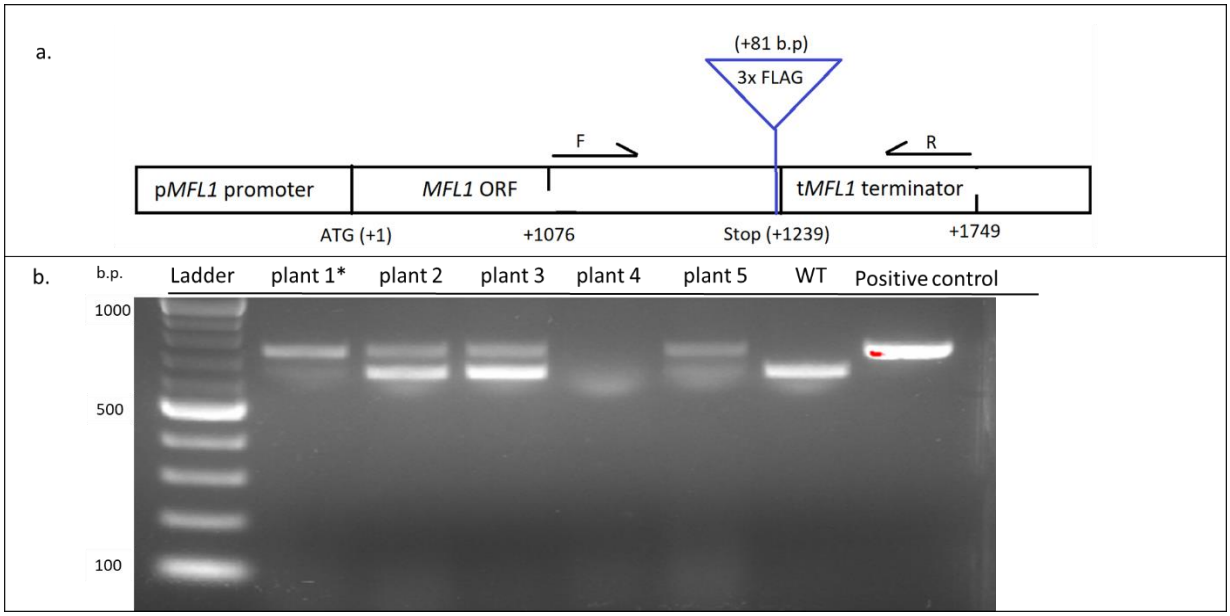

Figure 2.6. Complemented mfl1-2 mutants have an 81 base pair 3xFLAG tag in the C- terminal**.** (a.) The primers were designed to flank the 3xFLAG tags, the wildtype band is expected to be 764 base pairs, and the complemented lines have 845 base pairs, with F being the forward *mfl1* promoter primer and R being the reverse *mfl1* primer (Supplementary Table 1.). (b.) gel image of the PCR analysis verifying the complemented lines in mfl1-2 mutants. Plant 1, marked with an asterisk (*), is used in further experiments as (r7). The positive control is the MFL1 complementary plasmid (Supplementary Figure 2.).

To examine changes in the photorespiratory capacity of our transgenic *A. thaliana* plants, we compared their photorespiratory rate with a WT plant and a known photorespiratory mutant *plgg1* (Pick et al., 2013) under high and ambient CO_2 conditions. In a 30-day growth assay under high CO_2 conditions, all transgenic plants showed similar rosette leaf areas compared to the WT (Fig 2.7.).

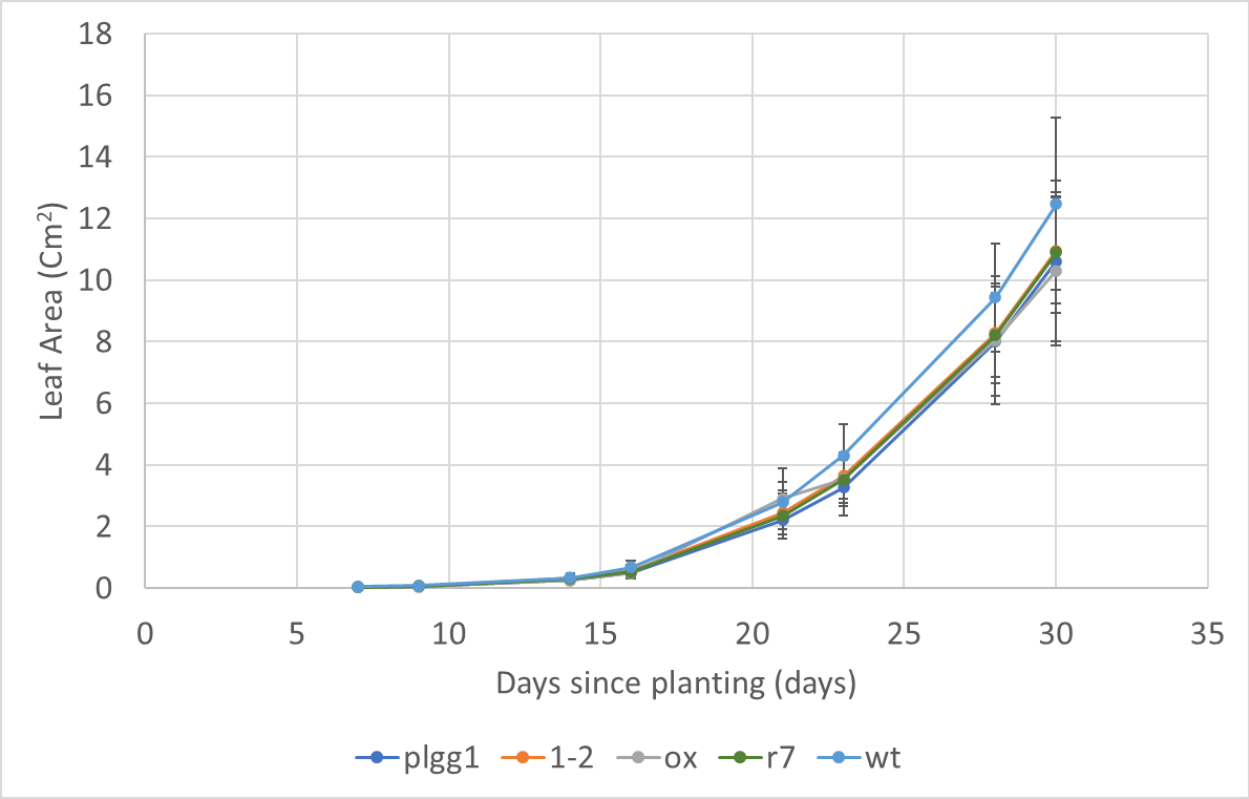

Figure 2.7. Transgenic plants have similar rosette areas in a high CO_2 environment. A 30-Day growth assay was performed on 12 samples of wildtype (wt), *mfl1-2(1-2)*, plgg*1*, Overexpression (ox), and rescue (r7). Data points show the average rosette size. Twelve plants were subjected to 2000 ppm CO_2. Error bars indicate a standard deviation from the average measurement.

In a 30-day growth assay under ambient CO_2 conditions, the *plgg1* plants had leaf rosettes smaller than those in WT. The *mfl1-2* plants had leaf rosettes smaller than those in WT but differences were not statistically significant (Fig. 2.8.). *A. thaliana* plants in both conditions on the 28th day were presented for visualization purposes (Fig. 2.9.).

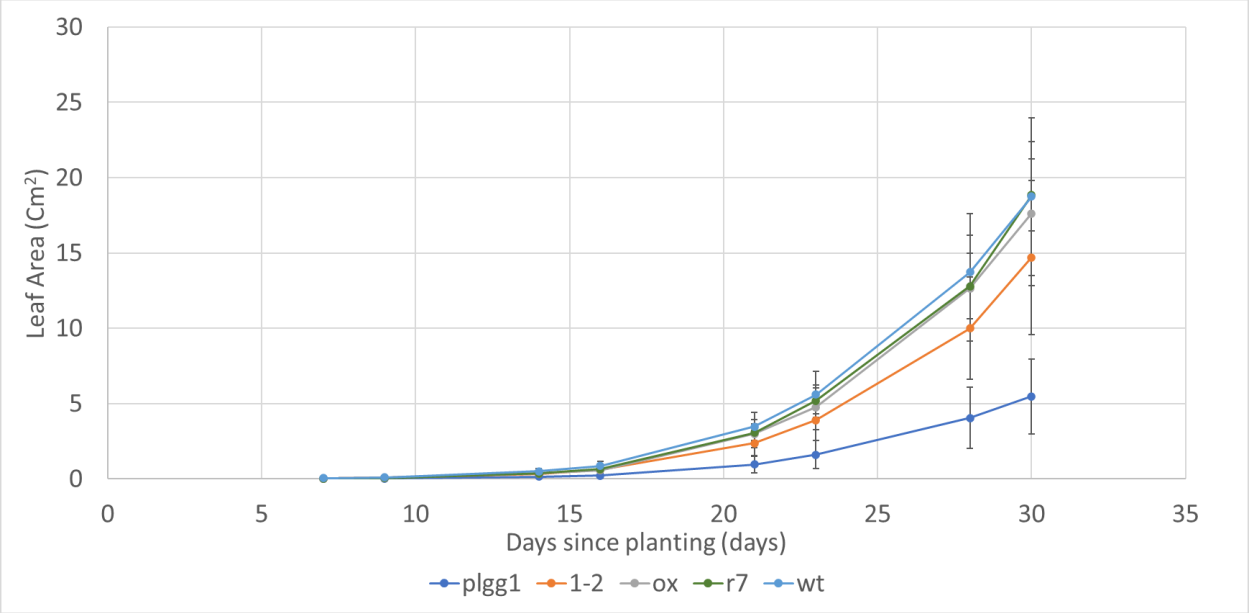

Figure 2.8. mfl1-2 mutants may have a smaller average rosette area compared to WT in an ambient CO_2 environment. A 30-Day growth assay was performed on 12 samples of wildtype (WT), *mfl1-2(1-2)*, *plgg1*, Overexpression (ox), and rescue (r7). Data points show the average rosette size. Twelve plants were subjected to ambient CO2. Error bars indicate a standard deviation from the average measurement.

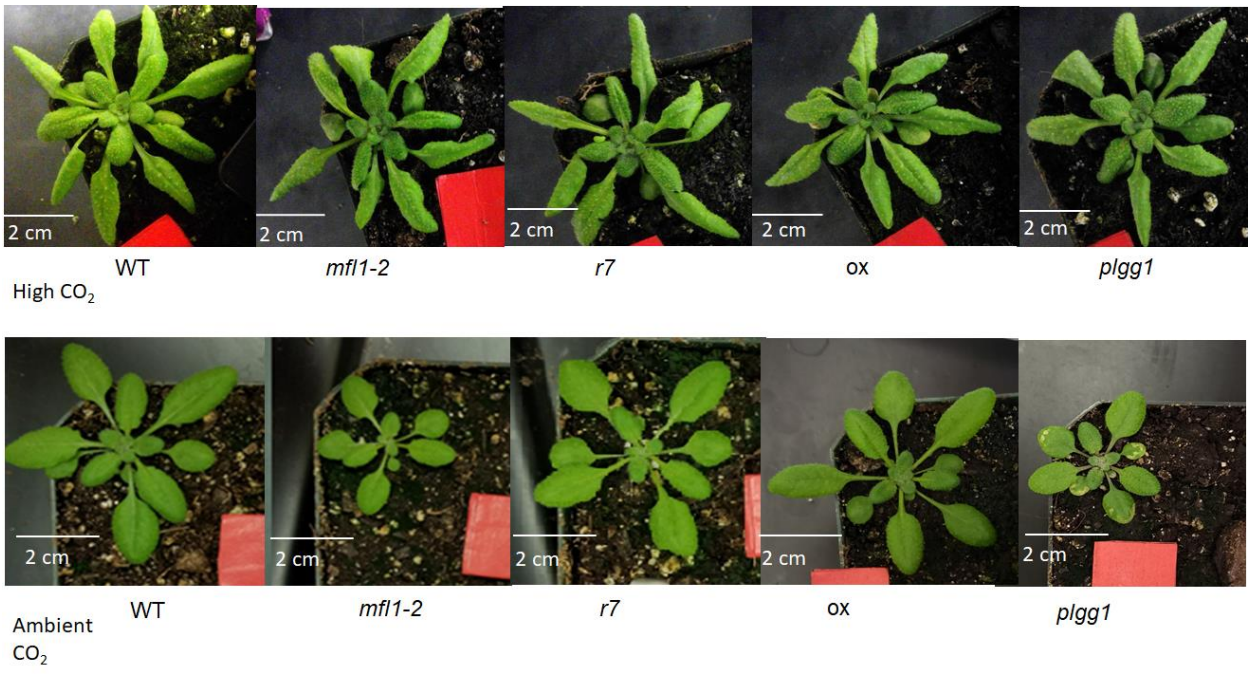

Figure 2.9. *mfl1-2* mutants may have a smaller rosette area compared to WT in ambient conditions**.** Representative leaf images of wildtype (WT), *mfl1-2*, rescue (r7) Overexpression (ox), and *plgg1* with high CO_2 (Top row) and ambient CO_2 (Bottom row) conditions. Images were taken on the 28th day.

Since the products of photorespiration, namely phosphoglycolate, inhibits the repair process of photoprotection that protects the plant from excess light (Takahashi et al., 2007; Takahashi & Murata, 2008), we would expect that photorespiration mutants would have a measurable alteration of the photochemical quenching process that protects the plant from excess light. Therefore, we conducted a nonphotochemical quenching experiment. Under ambient CO_2 conditions, there is no discernable difference in non-photochemical quenching effects between *mfl1-2* plants and WT plants (Fig. 2.10.)

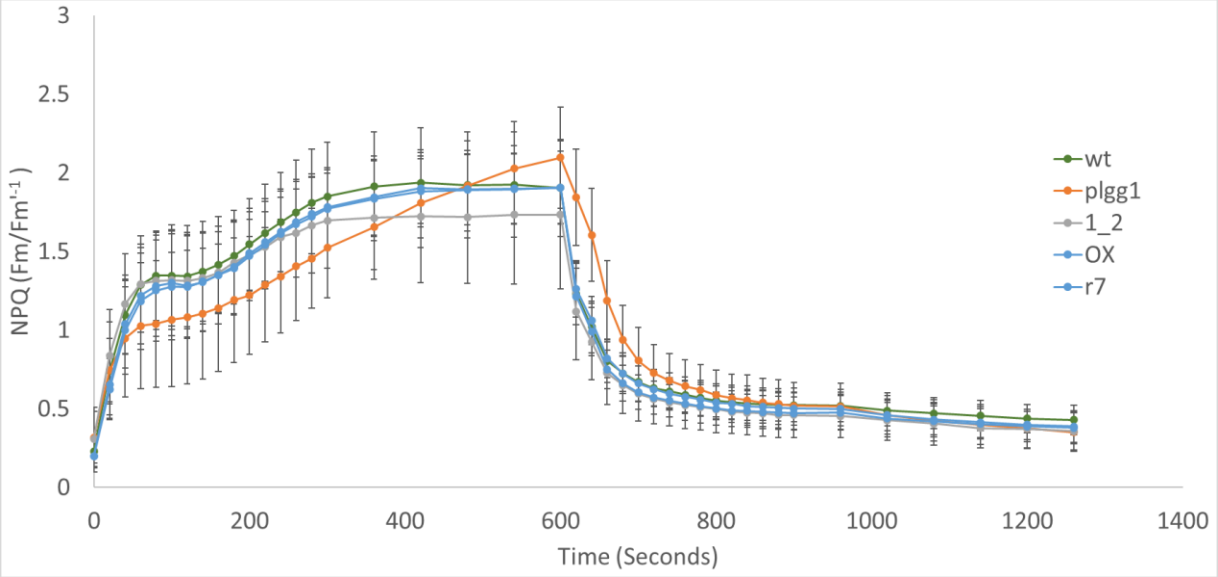

Figure 2.10. *mfl1-2* has a similar non-photochemical quenching (NPQ) profile compared to WT. 9-Day-old seedlings of wildtype (wt), *mfl1-2* (1_2), *plgg1*, overexpression (OX), and rescue (r7) lines were imaged for NPQ response. Data points show the average NPQ response. Plants were subjected to ambient CO_2. Error bars indicate standard deviation.

We then used yeast as a model organism to measure the iron transport activity of MFL1. The logic was that if the protein does transport this solute, it can rescue yeast that does not have its native transporter. In BY4742 yeast with its native iron transporter, FTR1 knocked out, there was a visual negative growth effect on the medium containing reduced iron. When *mfl1* is ectopically

expressed into either WT or *ftr1Δ* knockout yeast, no visual growth effect was observed (Fig. 2.11.). This suggested that MFL1 does not function as the iron transporter in yeast.

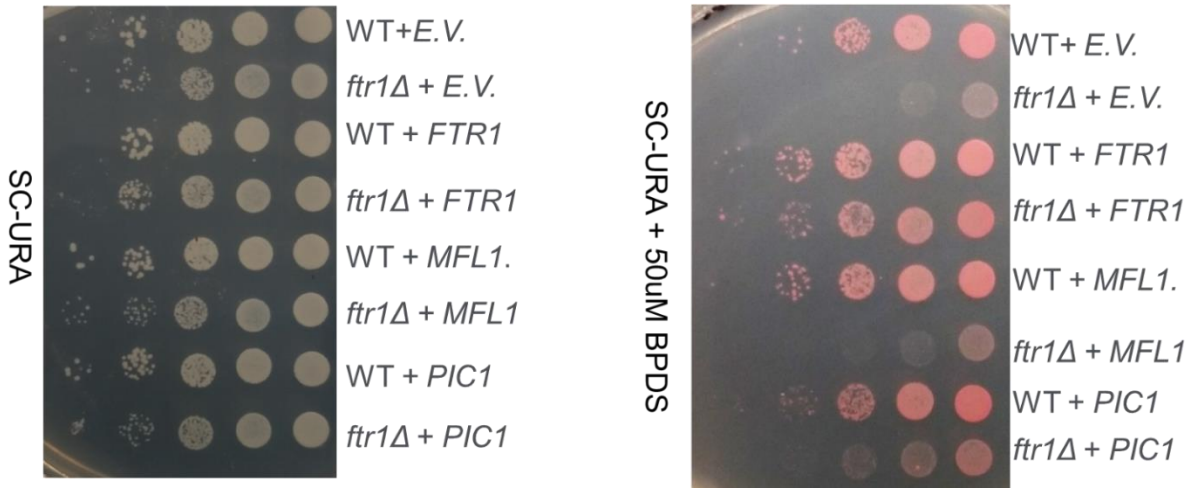

Figure 2.11. MFL1 has a negligible effect on Fe^{3+} transport in yeast. serial dilutions of WT and iron transporter knockout (*ftr1Δ*) yeast with empty vector (*E.V.*), FTR1, MFL1 or permease in chloroplast (*PIC1*) transporter protein. Ten µL yeast cultures (OD_{600} =0.1) in water were plated onto SC-URA plates with no additive (control, left), and bathophenanthrolinedisulfonate (BPDS) (experimental, right) with 4 to 10-fold serial dilutions. The plates were grown for 1d at 30°C.

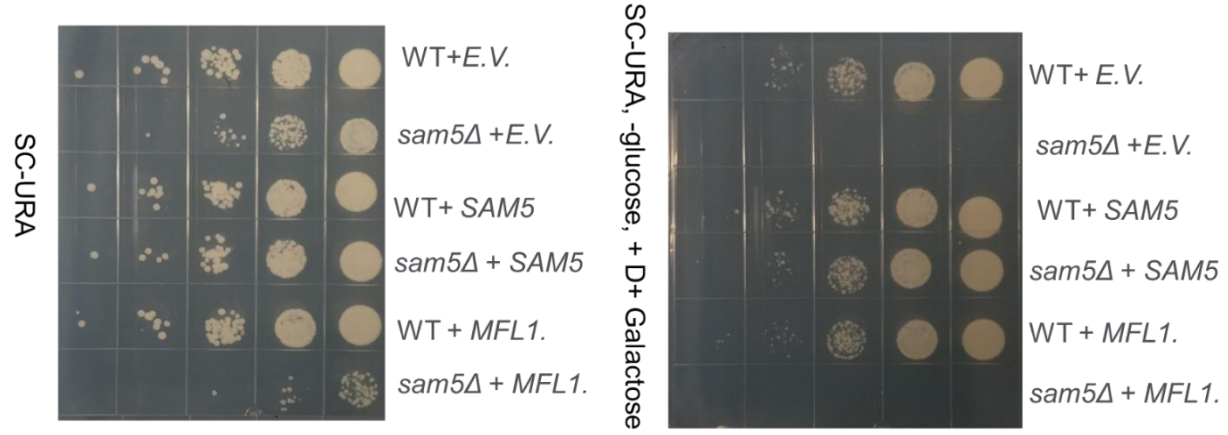

Figure 2.12. MFL1 has a detrimental effect on SAM transport in yeast. Serial dilutions of WT and S- adenosyl methionine transport knockout *(sam5Δ)* yeast with empty vector (*E.V.*), SAM5, and MFL1 transport protein. Ten µL yeast cultures (O.D.600 = 0.1) in water were spotted onto SC-URA plates with no additive (control, left), and glucose was replaced with D+ Galactose (experimental, right) with 4 - 10-fold serial dilutions. The plates were grown for 2d at 30°C.

We then evaluated MFL1's ability to transport SAM in a similar format. In BY4741 yeast with its native SAM transporter knocked out (*sam5Δ)*, there was a visual negative growth effect

on the medium containing a non-fermentation carbon source (galactose). When MFL1 was ectopically expressed into either WT or *sam5Δ* knockout yeast, no visual growth effect was observed (Fig. 2.12.).

2.4. Discussion

Our experiments did not suggest MFL1 was responsible for iron or SAM transport in *A. thaliana*. To examine the biological function of MFL1, we obtained seemingly knock-out mutant varieties of MFL1 and verified that their T-DNA insertion point was at the promoter region (Fig.4.). We then verified that the *mfl1-2* knockout mutants did indeed produce no RNA transcript, the logic being if there was no mRNA transcript being produced, there would not be any MFL1 protein produced. However, end-point PCR suggested the *mfl1-2* knockout mutants only reduced but not completely halted the expression of the *MFL1* gene. However, this yielded mutants that display a reduced expression (knockdown) phenotype instead of a complete knockout phenotype (Fig.5.). We also made mutant *A. thaliana* plants that had an overexpressed *MFL1* construct with a C-terminal eGFP tag inserted within the genome and verified with PCR (Fig. 6. and 7.). Under a high CO_2 environment, the sizes of rosette leaves in all transgenic plants are similar to those in wild type *A. thaliana.* (Fig. 8., Fig. 10.). However, under ambient CO_2, the *MFL1* mutants have a slightly reduced rosette size compared to the WT and rescue lines (Fig. 9., Fig. 10.). Because the reduced growth effect was statistically not significant as the photorespiratory impaired mutant *plgg1* (Cui et al., 2021), further analysis will be required to conclude the observation in this study. We also tried to identify the NPQ reaction time and capacity of *mfl1* mutants, but the mutants appear to have only a slight average reduction of NPQ capacity compared to WT (Fig. 11.). Further tests are needed since there was only one transgenic line tested. Another important experiment is needed to determine the expression of MFL1 protein

in transgenic plants compared to WT. Without the determination, the results obtained in this study remain preliminary.

MFL1 did not appear to rescue the iron transport ability when inserted into yeast (Fig. 12.). In yeast, the iron transporter FTR1 is located on the cell membrane and transports iron into the cell after it has been converted from Fe^{2+} to Fe^{3+} by the enzyme (Stearman et al., 1996). One reason MFL1 could not transport iron to rescue the mutant may be because MFL1 may transport Fe^{2+} instead of Fe^{3+} and further experiments would need to target Fe^{2+} instead of Fe^{3+}. MFL1 also did not appear to rescue yeast with reduced SAM transport ability in SC-URA galactose media (Fig.13.), In yeast, the SAM transporter PET8 serves a similar role of transporting SAM from the cytosol into the mitochondria (Marobbio et al., 2003). However, MFL1 seems to exacerbate the reduced growth phenotype in *sam5Δ* knockout yeast in SC-URA glucose media (Fig.13.). One possible explanation for the reduced growth phenotype could be that the MFL1 protein is inverted within the mitochondrial membrane in the yeast, so instead of importing SAM, it exports more of it out; further tests will be needed to verify that MFL1 does transport SAM. Another possibility is that even though MFL1 in the yeast experiment is codon optimized and under a yeast constitutive promoter, MFL1 may still not be expressed correctly in yeast.

CONCLUSION AND FUTURE DIRECTION

From our experiments, it would suggest that MFL1 may contrast with the previous literature that suggests MFL1 is responsible for iron transport into the chloroplast (Tarantino et al., 2011). Although we used *A. thaliana* as the model organism to study MFL1, proteins similar to MFL1 may also exist in other photosynthetic organisms that may play a similar role in balancing the chemical reaction necessary to maintain photosynthesis in its optimal state and buffer for sudden chemical imbalances. Although we used *S. cerevisiae* as a model organism to determine MFL1's substrate, future experiments could be to use radiolabeled SAM evaluated in an uptake assay similar to the procedure outlined in a previous study (South et al., 2017). Another possible experiment to visually identify the location of MFL1 within the chloroplast is by using eGFP-tagged MFL1 and inserting them into Arabidopsis or *N. benthamiana* protoplasts and observing where the eGFP fluorescence is occurring within the cell.

Understanding the biochemical pathways of photosynthesis is important, but we will also need to know how the molecules are moved into and out of the compatibilized organelles past the double membrane and delivered in the appropriate quantities to maintain the stoichiometry balance necessary for the function of the cell. Further directions to explore the function of MFL1 and its role in photorespiration could be to see how knockdown plants perform in a low carbon dioxide environment and use radioactive labeling to determine the substrate MFL1 transports. Understanding the role of MFL1 could lead to improvements in photorespiration and alternative pathways in photosynthesis in analogous transporters of other species.

APPENDIX A. SUPPLEMENTARY TABLES

Supplementary Table 1. List of primers used in this experiment.

Sequence	Name	Gene	Organism	Function
TGGCTCTAGGCGATGGAACT	pAtMFL1-1006F	MFL1	Arabidopsis	verify presense of MFL1 promoter (left border)
AACATGGTGGTCAGAGAATCG	SALK_007617_LP2	MFL1	Arabidopsis	verify MFL1 knockout inserts (left border)
TTGATCCATTTCAGGAATTCG	SALK_007617_RP2	MFL1	Arabidopsis	verify MFL1 knockout inserts (right border)
ATTTTGCCGATTTCGGAAC	Lba1.3	T-DNA insert	Arabidopsis	confirm presence of T-DNA in KO plants (Left border)
CGTTCCCAGACGGAGAGTTG	Atmfl_318 R	MFL1	Arabidopsis	verify presense of MFL1 promoter (right border)
AGGTTGGGTTGGTTTTACCC	AtMFL1-seq 1201F	MFL1	Arabidopsis	verify presense of MFL1 gene (left border)
GACTCTCCGAAACTCTTGGC	AtMFL1_EP_3F	MFL1	Arabidopsis	Primer used in endpoint pcr (left border)
GGCAAAATAACCGATCGCAG	AtMFL1_EP_3R	MFL1	Arabidopsis	Primer used in endpoint pcr (right border)
TGAGTTCAACGAGTGTGCTG	VDE-RT-1F	VDE	Arabidopsis	Primer used in endpoint pcr (left border)
ACTTGTAATGTACCACTTCCCG	VDE-RT-2R	VDE	Arabidopsis	Primer used in endpoint pcr (right border)
ATAACCGCGAGATAGAGAGGC	PLGG1F genotypying primer	PLGG1	Arabidopsis	Genotypying for T-DNA insertion (left border)
CCCATGGCTACTCTTTTAGCC	PLGG1R genotypying primer	PLGG1	Arabidopsis	Genotypying for T-DNA insertion (right border)
AAGATCTCTCTGCCGACAGT	p35s-seq -186F	p35	Arabidopsis	sanger sequencing primer for p35 promoter (left border)
TCTGACGATAGGGCTTTGGA	AtMFL1-seq 237R	Atmfl1	Arabidopsis	sanger sequencing primer for MFL1 (right border)
AGGTTGGGTTGGTTTTACCC	AtMFL1-seq 1201F	atmfl1	Arabidopsis	sanger sequencing primer for MFL1 (left border)
GATGAACTTCAGGGTCAGCT	EC16570 eGFP-seq 128R	eGFP	Arabidopsis	sanger sequencing primer for C-terminal eGFP tag (right border)
TCAAGATCCGCCACAACATC	EC16570 eGFP-seq 500F	eGFP	Arabidopsis	sanger sequencing primer for C-terminal eGFP tag (left border)
TCAACACATGAGCGAAACCC	t35s-seq 85R	t35s	Arabidopsis	sanger sequencing primer for t35 terminator (left border)
GCTGTAGTTCGACCTTGAGC	PFTRP YO 1F	ftr1p	Yeast	verify presense of yeast ftr1p promoter (left border)
CGGGAGGCTGAATCAAGAAC	PSAM yo 1f	sam5	Yeast	verify presense of yeast SAM5 promoter (left border)
GAGTCGGCTTTAACGTGGAG	Ftr1p-yo-1r	ftr1p	Yeast	verify presense of yeast ftr1p promoter (right border)
CTCATTTCTCCAGCCGTTGG	SAM5_YO 1r	sam5	Yeast	verify presense of yeast SAM5 promoter (right border)
CATTCGCATCCACGAGCATC	Atmfl_yo_1f	MFL1	Yeast	verify presense of yeast optimized MFL1 (left border)
GTCTCGAATGCGAAGTACCC	Atmfl_y0_1r	MFL1	Yeast	verify presense of yeast optimized MFL1 (right border)
CGTGAGTCTTTTCCTTACCC	y_KanMX_1F	KanMX	Yeast	verify presense of yeast Kanamycin resistance(left border)
TTTGATGCTCGATGAGTTTTTC	y_KanMx_1R	KanMX	Yeast	verify presense of yeast Kanamycin resistance(right border)
GTTGGCCTTGTCTGTACG	y_ftr1p_2F	FTR1P	Yeast	verify presense of yeast ftr1p gene (left border)
CGTACAGACAAGGCCAAC	y_ftr1p_2r	FTR1P	Yeast	verify presense of yeast ftr1p gene (right border)
CTAAGGGTGGATTCTTTGCTAAT	y_SAM5_2F	sam5	Yeast	verify presense of yeast SAM5 gene (left border)
AGAAGACTGTGAAAAGAGTCTG	y_SAM5_2r	sam5	Yeast	verify presense of yeast SAM5 gene (right border)
GGGACATATCACGGCCA	yeast_TUB2_1F	TUB2	Yeast	verify presense of yeast TUB2 gene (left border)
CCTCTTGGTATTGTTGGTATTCG	yeast_TUB2_1R	TUB2	Yeast	verify presense of yeast TUB2 gene (right border)
GCAAATGCCTGCAAATCGC	TADH1 F	ADH1	Yeast	verify yeast MoClo plasmids (left border)
ATTCTGCTGTAACCCGTACAT	PTDH3	tdh3	Yeast	verify yeast MoClo plasmids (right border)

Supplementary Table 2. List of yeast inserts combinations.

name	promoter	gene	signal	C-terminal tag
pjq004	TDH3 promoter (PYTK003)	MFL1 CDS	MFL1	N/A
pjq005	FTRP promoter	Ftr1p	MFL1	N/A
pjq006	SAM5 promoter	SAM5 CDS	MFL1	N/A
pjq007	SAM5 promoter	MFL1 CDS	MFL1	N/A
pjq008	FTRP promoter	MFL1 CDS	MFL1	N/A
pjq009	TDH3 promoter (PYTK003)	MFL1 CDS	FTR1P	N/A
pjq010	TDH3 promoter (PYTK003)	MFL1 CDS	SAM5	N/A
pjq011	FTRP promoter	MFL1 CDS	SAM5	N/A
pjq012	SAM5 promoter	MFL1 CDS	SAM5	N/A
pjq013	TDH3 promoter (PYTK003)	MFL1 CDS	MFL1	3XFLAG
pjq014	FTRP promoter	MFL1 CDS	FTR1P	3XFLAG
pjq015	SAM5 promoter	MFL1 CDS	SAM5	3XFLAG

Supplementary Table 3. Yeast media components

SC-URA (chemic al and ammino acid mix)	ingredients	concentration (mg/L)
	Adenine hemisulfate	21
	L-Alanine	85.6
	L-Arginine	85.6
	L-Asparagine monohydrate	85.6
	L-Aspartic acid	85.6
	L-Cysteine hydrochloride monohydrate	85.6
	L-Glutamic acid	85.6
	L-Glutamine	85.6
	L-Glycine	85.6
	L-Histidine hydrochloride monohydrate	85.6
	Inositol	85.6
	L-Isoleucine	85.6
	L-Leucine	173.4
	L-Lysine hydrochloride	85.6
	L-Methionine	85.6
	4-Aminobenzoic acid (PABA)	8.6
	L-Phenylalanine	85.6
	L-Proline	85.6
	L-Serine	85.6
	L-Threonine	85.6
	L-Tryptophan	85.6
	L-Tyrosine	85.6
	L-Valine	85.6
SC-URA growth plates (1L)	components	Amounts
	YNB	1.71g
	Sc-ura	1.2g
	Glucose (2%)	20g
	Ammonium sulfate	5g
	agarose	14 g
SC-URA replaced with glycerol (1L)	components	Amounts
	YNB	1.71g
	Sc-ura	1.2g
	Glycerol (3%)	30 ml
	Ammonium sulfate	5g

APPENDIX B. SUPPLEMENTARY FIGURES

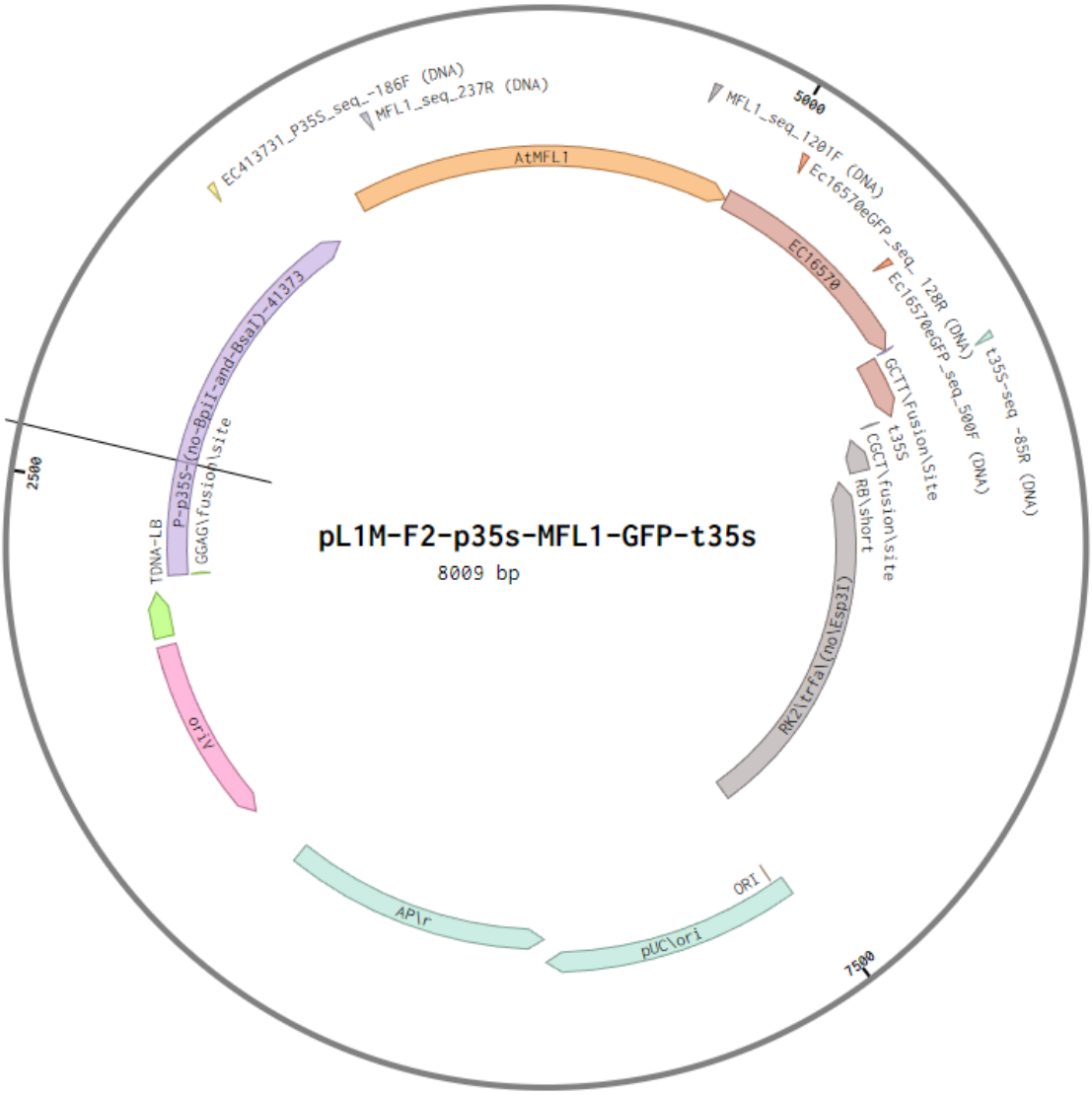

Supplementary Figure 1. Golden Gate level 1 plasmid layout for p35 MFL1 overexpression lines EC16570: C-terminal eGFP tag.

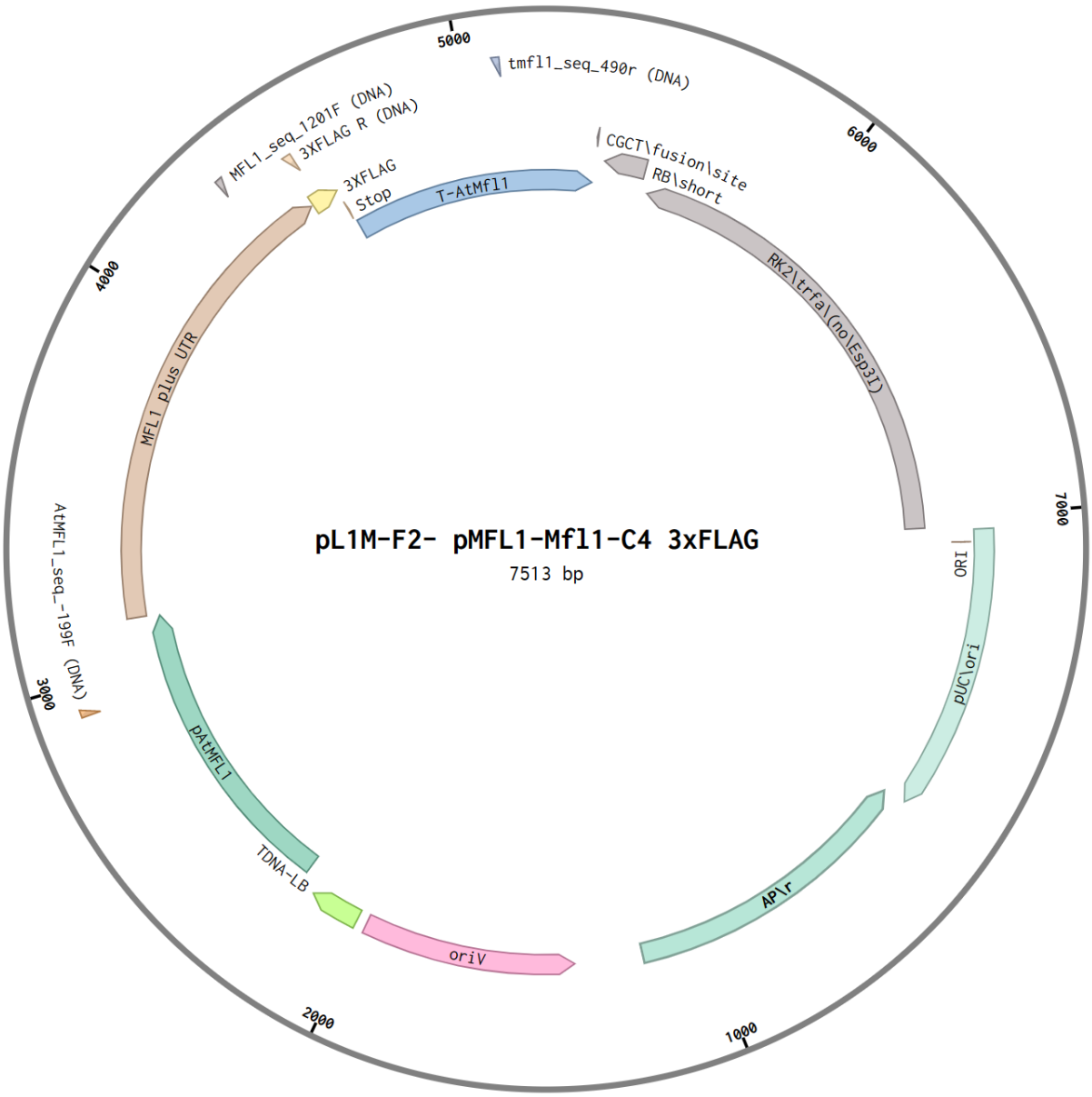

Supplementary Figure 2. Golden Gate level 1 plasmid layout for complementary MFL1 lines.

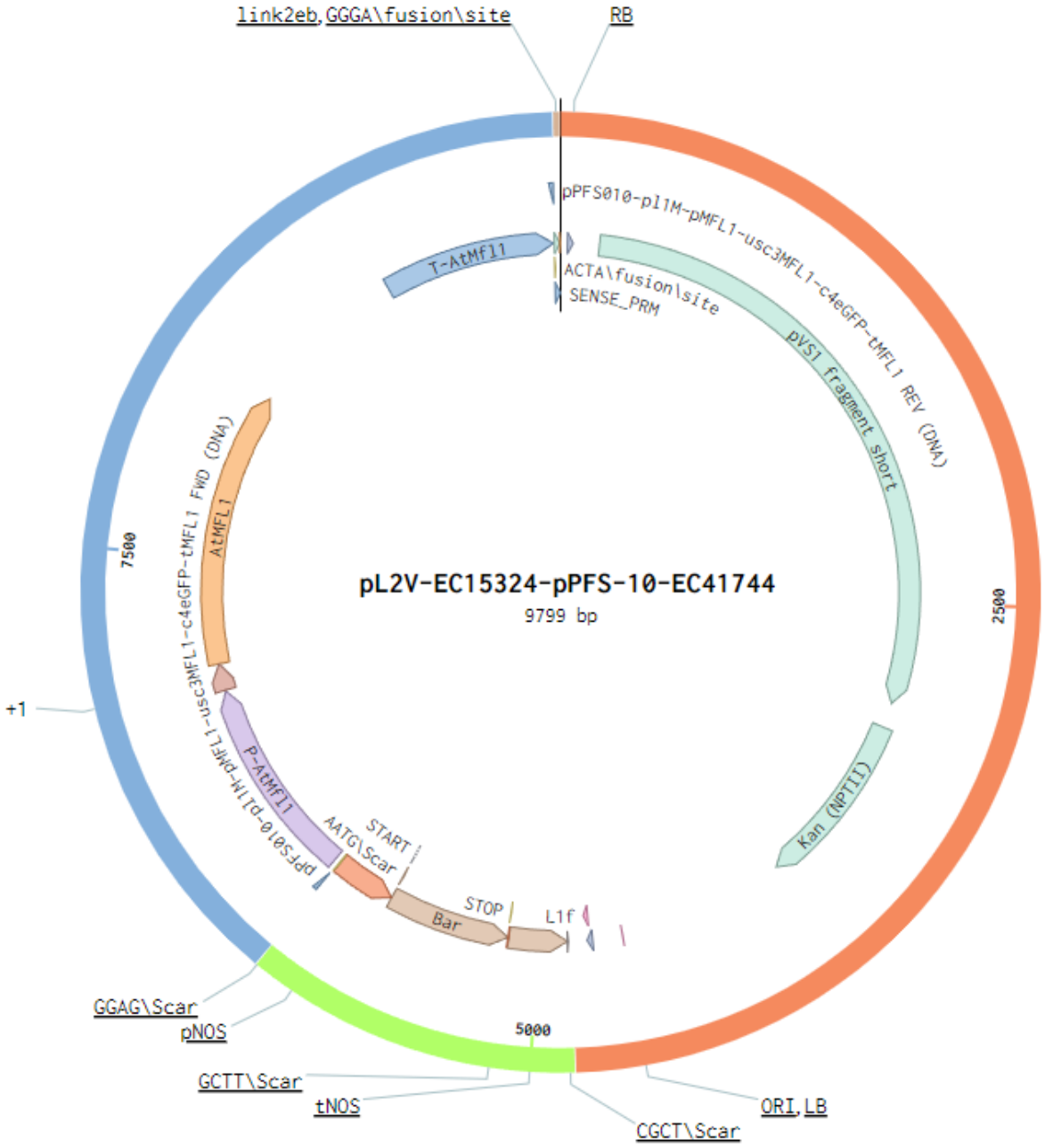

Supplementary Figure 3. Golden Gate level 2 plasmid layout for complementary MFL1 lines.

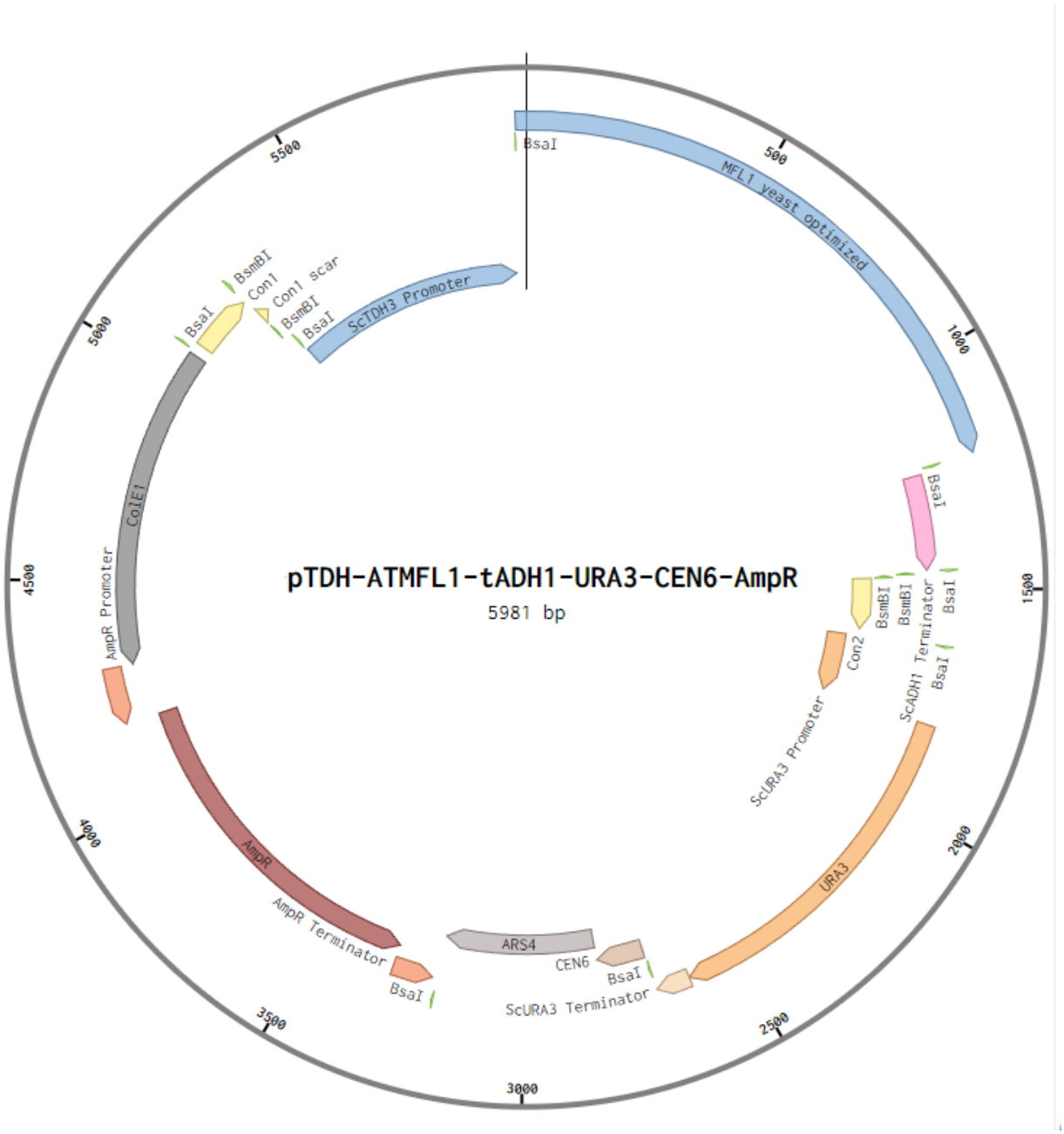

Supplementary Figure 4. Yeast MoClo plasmid layout

REFERENCES

Amesz, J. (1973). The function of plastoquinone in photosynthetic electron transport. *Biochimica et Biophysica Acta (BBA)-Reviews on Bioenergetics*, *301*(1), 35-51.

Andersen, B., Scheller, H. V., & Møller, B. L. (1992). The PSI-E subunit of photosystem I binds ferredoxin: NADP+ oxidoreductase. *FEBS letters*, *311*(2), 169-173.

Anderson, L. E. (1971). Chloroplast and cytoplasmic enzymes II. Pea leaf triose phosphate isomerases. *Biochimica et Biophysica Acta (BBA)-Enzymology*, *235*(1), 237-244.

Arnon, D. I. (1971). The light reactions of photosynthesis. *Proceedings of the National Academy of Sciences*, *68*(11), 2883-2892.

Bashir, K., Ishimaru, Y., Shimo, H., Nagasaka, S., Fujimoto, M., Takanashi, H., . . . Nishizawa, N. K. (2011). The rice mitochondrial iron transporter is essential for plant growth. *Nature communications*, *2*(1), 322.

Bassham, J. A. (2005). Mapping the carbon reduction cycle: a personal retrospective. *Discoveries in photosynthesis*, 817-832.

Beckmann, K., Dzuibany, C., Biehler, K., Fock, H., Hell, R., Migge, A., & Becker, T. W. (1997). Photosynthesis and fluorescence quenching, and the mRNA levels of plastidic glutamine synthetase or of mitochondrial serine hydroxymethyltransferase (SHMT) in the leaves of the wild-type and of the SHMT-deficient stm mutant of Arabidopsis thaliana in relation to the rate of photorespiration. *Planta*, *202*, 379-386.

Campbell, W. H., & Redinbaugh, M. G. (1984). Ferric-citrate reductase activity of nitrate reductase and it's role in iron assimilation by plants. *Journal of Plant Nutrition*, *7*(1-5), 799-806.

Cui, L., Zhang, C., Li, Z., Xian, T., Wang, L., Zhang, Z., . . . Peng, X. (2021). Two plastidic glycolate/glycerate translocator 1 isoforms function together to transport photorespiratory glycolate and glycerate in rice chloroplasts. *Journal of Experimental Botany*, *72*(7), 2584-2599.

Duy, D., Wanner, G., Meda, A. R., von Wiren, N., Soll, J., & Philippar, K. (2007). PIC1, an ancient permease in Arabidopsis chloroplasts, mediates iron transport. *The Plant Cell*, *19*(3), 986-1006.

Easlon, H., & Bloom, A. (2014). Easy Leaf Area: Automated Digital Image Analysis for Rapid and Accurate Measurement of Leaf Area. Applications in Plant Sciences. In.

Flügel, F., Timm, S., Arrivault, S., Florian, A., Stitt, M., Fernie, A. R., & Bauwe, H. (2017). The photorespiratory metabolite 2-phosphoglycolate regulates photosynthesis and starch accumulation in Arabidopsis. *The Plant Cell*, *29*(10), 2537-2551.

Hall, D., Rao, K., & Cammack, R. (1975). The iron-sulphur proteins: structure, function and evolution of a ubiquitous group of proteins. *Science Progress (1933-)*, 285-317.

Hirabayashi, K., Yuda, E., Tanaka, N., Katayama, S., Iwasaki, K., Matsumoto, T., . . . Takahashi, Y. (2015). Functional dynamics revealed by the structure of the SufBCD complex, a novel ATP-binding cassette (ABC) protein that serves as a scaffold for iron-sulfur cluster biogenesis. *Journal of Biological Chemistry*, *290*(50), 29717-29731.

Hu, X., Kato, Y., Sumida, A., Tanaka, A., & Tanaka, R. (2017). The SUFBC 2D complex is required for the biogenesis of all major classes of plastid Fe-S proteins. *The Plant Journal*, *90*(2), 235-248.

Igarashi, D., Miwa, T., Seki, M., Kobayashi, M., Kato, T., Tabata, S., . . . Ohsumi, C. (2003). Identification of photorespiratory glutamate: glyoxylate aminotransferase (GGAT) gene in Arabidopsis. *The Plant Journal*, *33*(6), 975-987.

Kelley, L. A., Mezulis, S., Yates, C. M., Wass, M. N., & Sternberg, M. J. (2015). The Phyre2 web portal for protein modeling, prediction, and analysis. *Nature protocols*, *10*(6), 845-858.

Kelly, G., & Latzko, E. (1976). Inhibition of spinach-leaf phosphofructokinase by 2-phosphoglycollate. *FEBS letters*, *68*(1), 55-58.

Kurisu, G., Zhang, H., Smith, J. L., & Cramer, W. A. (2003). Structure of the cytochrome b6f complex of oxygenic photosynthesis: tuning the cavity. *Science*, *302*(5647), 1009-1014.

Lee, M. E., DeLoache, W. C., Cervantes, B., & Dueber, J. E. (2015). A Highly Characterized Yeast Toolkit for Modular, Multipart Assembly. *ACS Synth Biol*, *4*(9), 975-986. https://doi.org/10.1021/sb500366v

Liepman, A. H., & Olsen, L. J. (2003). Alanine aminotransferase homologs catalyze the glutamate: glyoxylate aminotransferase reaction in peroxisomes of Arabidopsis. *Plant Physiology*, *131*(1), 215-227.

Marobbio, C., Agrimi, G., Lasorsa, F., & Palmieri, F. (2003). Identification and functional reconstitution of yeast mitochondrial carrier for S-adenosylmethionine. *The EMBO journal*, *22*(22), 5975-5982.

Marsh, J. J., & Lebherz, H. G. (1992). Fructose-bisphosphate aldolases: an evolutionary history. *Trends in biochemical sciences*, *17*(3), 110-113.

Meneghin, E., Volpato, A., Cupellini, L., Bolzonello, L., Jurinovich, S., Mascoli, V., . . . Collini, E. (2018). Coherence in carotenoid-to-chlorophyll energy transfer. *Nat Commun*, *9*(1), 3160. https://doi.org/10.1038/s41467-018-05596-5

Pascal, A. A., Liu, Z., Broess, K., van Oort, B., van Amerongen, H., Wang, C., . . . Ruban, A. (2005). Molecular basis of photoprotection and control of photosynthetic light-harvesting. *Nature*, *436*(7047), 134-137. https://doi.org/10.1038/nature03795

Peterhansel, C., Horst, I., Niessen, M., Blume, C., Kebeish, R., Kürkcüoglu, S., & Kreuzaler, F. (2010). Photorespiration. *The arabidopsis book*, *2010*(8).

Pick, T. R., Bräutigam, A., Schulz, M. A., Obata, T., Fernie, A. R., & Weber, A. P. (2013). PLGG1, a plastidic glycolate glycerate transporter, is required for photorespiration and defines a unique class of metabolite transporters. *Proceedings of the National Academy of Sciences*, *110*(8), 3185-3190.

Pilon-Smits, E. A., Garifullina, G. F., Abdel-Ghany, S., Kato, S.-I., Mihara, H., Hale, K. L., . . . Pilon, M. (2002). Characterization of a NifS-like chloroplast protein from Arabidopsis. Implications for its role in sulfur and selenium metabolism. *Plant Physiology*, *130*(3), 1309-1318.

Pintard, L., Bujnicki, J. M., Lapeyre, B., & Bonnerot, C. (2002). MRM2 encodes a novel yeast mitochondrial 21S rRNA methyltransferase. *The EMBO journal*, *21*(5), 1139-1147.

Porter, M. A., Milanez, S., Stringer, C. D., & Hartman, F. C. (1986). Purification and characterization of ribulose-5-phosphate kinase from spinach. *Archives of biochemistry and biophysics*, *245*(1), 14-23.

Rabinowitch, E. (1957). Photosynthesis and energy transfer. *The Journal of Physical Chemistry*, *61*(7), 870-878.

Ravanel, S., Block, M. A., Rippert, P., Jabrin, S., Curien, G., Rébeillé, F., & Douce, R. (2004). Methionine metabolism in plants: chloroplasts are autonomous for de novo methionine synthesis and can import S-adenosylmethionine from the cytosol. *Journal of Biological Chemistry*, *279*(21), 22548-22557.

Ravet, K., Touraine, B., Boucherez, J., Briat, J. F., Gaymard, F., & Cellier, F. (2009). Ferritins control interaction between iron homeostasis and oxidative stress in Arabidopsis. *The Plant Journal*, *57*(3), 400-412.

Saini, A., Mapolelo, D. T., Chahal, H. K., Johnson, M. K., & Outten, F. W. (2010). SufD and SufC ATPase activity are required for iron acquisition during in vivo Fe-S cluster formation on SufB. *Biochemistry*, *49*(43), 9402-9412.

Santamaría, E., Avila, M. A., Latasa, M. U., Rubio, A., Martín-Duce, A., Lu, S. C., . . . Corrales, F. J. (2003). Functional proteomics of nonalcoholic steatohepatitis: mitochondrial proteins as targets of S-adenosylmethionine. *Proceedings of the National Academy of Sciences*, *100*(6), 3065-3070.

Solti, Á., Müller, B., Czech, V., Sárvári, É., & Fodor, F. (2014). Functional characterization of the chloroplast ferric chelate oxidoreductase enzyme. *New Phytologist*, *202*(3), 920-928.

South, P. F., Walker, B. J., Cavanagh, A. P., Rolland, V., Badger, M., & Ort, D. R. (2017). Bile acid sodium symporter BASS6 can transport glycolate and is involved in photorespiratory metabolism in Arabidopsis thaliana. *The Plant Cell*, *29*(4), 808-823.

Stearman, R., Yuan, D. S., Yamaguchi-Iwai, Y., Klausner, R. D., & Dancis, A. (1996). A permease-oxidase complex involved in high-affinity iron uptake in yeast. *Science*, *271*(5255), 1552-1557.

Steinberg-Yfrach, G., Rigaud, J.-L., Durantini, E. N., Moore, A. L., Gust, D., & Moore, T. A. (1998). Light-driven production of ATP catalysed by F0F1-ATP synthase in an artificial photosynthetic membrane. *Nature*, *392*(6675), 479-482.

Tabita, F. R., Hanson, T. E., Li, H., Satagopan, S., Singh, J., & Chan, S. (2007). Function, structure, and evolution of the RubisCO-like proteins and their RubisCO homologs. *Microbiology and Molecular Biology Reviews*, *71*(4), 576-599.

Takahashi, S., Bauwe, H., & Badger, M. (2007). Impairment of the photorespiratory pathway accelerates photoinhibition of photosystem II by suppression of repair but not acceleration of damage processes in Arabidopsis. *Plant Physiology*, *144*(1), 487-494.

Takahashi, S., & Murata, N. (2008). How do environmental stresses accelerate photoinhibition? *Trends in plant science*, *13*(4), 178-182.

Tarantino, D., Morandini, P., Ramirez, L., Soave, C., & Murgia, I. (2011). Identification of an Arabidopsis mitoferrinlike carrier protein involved in Fe metabolism. *Plant Physiology and Biochemistry*, *49*(5), 520-529. https://doi.org/10.1016/j.plaphy.2011.02.003

Thomas, P. D. (2010). GIGA: a simple, efficient algorithm for gene tree inference in the genomic age. *BMC bioinformatics*, *11*(1), 1-19.

Timm, S., Nunes-Nesi, A., Parnik, T., Morgenthal, K., Wienkoop, S., Keerberg, O., . . . Bauwe, H. (2008). A cytosolic pathway for the conversion of hydroxypyruvate to glycerate during photorespiration in Arabidopsis. *The Plant Cell*, *20*(10), 2848-2859.

Timm, S., Woitschach, F., Heise, C., Hagemann, M., & Bauwe, H. (2019). Faster removal of 2-phosphoglycolate through photorespiration improves abiotic stress tolerance of Arabidopsis. *Plants*, *8*(12), 563.

Weber, E., Engler, C., Gruetzner, R., Werner, S., & Marillonnet, S. (2011). A modular cloning system for standardized assembly of multigene constructs. *PloS one*, *6*(2), e16765.

Woodson, J. D., Perez-Ruiz, J. M., & Chory, J. (2011). Heme synthesis by plastid ferrochelatase I regulates nuclear gene expression in plants. *Current Biology*, *21*(10), 897-903.

Zelitch, I., Schultes, N. P., Peterson, R. B., Brown, P., & Brutnell, T. P. (2009). High glycolate oxidase activity is required for survival of maize in normal air. *Plant Physiology*, *149*(1), 195-204.

Zhang, H., Primak, A., Cape, J., Bowman, M. K., Kramer, D. M., & Cramer, W. A. (2004). Characterization of the high-spin heme x in the cytochrome b 6 f complex of oxygenic photosynthesis. *Biochemistry*, *43*(51), 16329-16336.

Zhang, P., Berardini, T. Z., Ebert, D., Li, Q., Mi, H., Muruganujan, A., . . . Thomas, P. D. (2020). PhyloGenes: An online phylogenetics and functional genomics resource for plant gene function inference. *Plant Direct*, *4*(12), e00293.

Zhang, X., Henriques, R., Lin, S.-S., Niu, Q.-W., & Chua, N.-H. (2006). Agrobacterium-mediated transformation of Arabidopsis thaliana using the floral dip method. *Nature protocols*, *1*(2), 641-646.

VITA

Joseph Qian was born in 1997 in Alhambra, California. He obtained his high school diploma in 2016 from University High School in Irvine, California. For his undergraduate work, he went to Emory University in Atlanta, Georgia. While there he deferred one semester to work at Bigelow Laboratory for Ocean Science for one semester and graduated from Emory University in 2019. In the Spring of 2020, he elected to obtain a graduate degree in Biochemistry at LSU and he is currently a candidate for the degree of Master of Science in the Department of Biochemistry, which is anticipated in May of 2023.